Article

Cell Reports

Inhibition of ERRα Prevents Mitochondrial Pyruvate Uptake Exposing NADPH-Generating Pathways as Targetable Vulnerabilities in Breast Cancer

Graphical Abstract

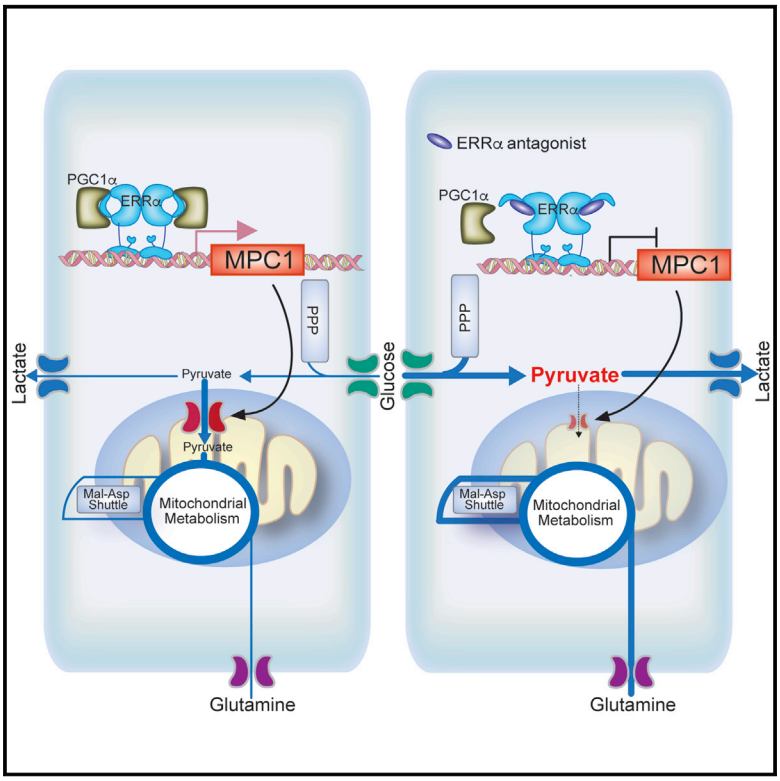

Authors

Sunghee Park, Rachid Safi, Xiaojing Liu, ..., Jason W. Locasale, Ching-yi Chang, Donald P. McDonnell

Correspondence

donald.mcdonnell@duke.edu

In Brief

Park et al. demonstrate that inhibition of mitochondrial metabolism can be accomplished using small molecule inhibitors of ERRα. Inhibiting the activity of this receptor decreases the expression of MPC1, interferes with pyruvate entry into the mitochondria, and increases cellular reliance on glutamine oxidation and the pentose phosphate pathway (PPP) to maintain NADPH homeostasis.

Highlights

- ERRα upregulates MPC1 expression to facilitate pyruvate entry into mitochondria
- ERRα inhibition introduces exploitable metabolic vulnerabilities into cancer cells
- Inhibition of ERRα increases reliance on glutamine oxidation and PPP to maintain NADPH
- ERRα antagonists increase the efficacy of GLS1 and G6PD inhibitors

Park et al., 2019, Cell Reports 27, 3587–3601
June 18, 2019 © 2019 The Author(s).
https://doi.org/10.1016/j.celrep.2019.05.066

CellPress

Cell Reports
Article

OPEN ACCESS
CellPress

Inhibition of ERRα Prevents Mitochondrial Pyruvate Uptake Exposing NADPH-Generating Pathways as Targetable Vulnerabilities in Breast Cancer

Sunghee Park,[1] Rachid Safi,[1] Xiaojing Liu,[1] Robert Baldi,[1] Wen Liu,[1] Juan Liu,[1] Jason W. Locasale,[1] Ching-yi Chang,[1] and Donald P. McDonnell[1,2,*]
[1]Department of Pharmacology and Cancer Biology, Duke University School of Medicine, Durham, NC 27710, USA
[2]Lead Contact
*Correspondence: donald.mcdonnell@duke.edu
https://doi.org/10.1016/j.celrep.2019.05.066

SUMMARY

Most cancer cells exhibit metabolic flexibility, enabling them to withstand fluctuations in intratumoral concentrations of glucose (and other nutrients) and changes in oxygen availability. While these adaptive responses make it difficult to achieve clinically useful anti-tumor responses when targeting a single metabolic pathway, they can also serve as targetable metabolic vulnerabilities that can be therapeutically exploited. Previously, we demonstrated that inhibition of estrogen-related receptor alpha (ERRα) significantly disrupts mitochondrial metabolism and that this results in substantial antitumor activity in animal models of breast cancer. Here we show that ERRα inhibition interferes with pyruvate entry into mitochondria by inhibiting the expression of mitochondrial pyruvate carrier 1 (MPC1). This results in a dramatic increase in the reliance of cells on glutamine oxidation and the pentose phosphate pathway to maintain nicotinamide adenine dinucleotide phosphate (NADPH) homeostasis. In this manner, ERRα inhibition increases the efficacy of glutaminase and glucose-6-phosphate dehydrogenase inhibitors, a finding that has clinical significance.

INTRODUCTION

Aerobic glycolysis has long been considered a dominant metabolic pathway in cancer cells, a conclusion reinforced by the observation that oncogene activation or loss of tumor suppressors results in a dramatic upregulation of glycolysis (Dang et al., 2011; Vander Heiden and DeBerardinis, 2017). Not surprisingly, therefore, there has been considerable interest in developing approaches to target those steps in glycolysis upon which cancer cells are most reliant (Dang et al., 2011). This approach has been somewhat successful although the therapeutic efficacy of drugs targeting glycolysis is limited by the inherent metabolic flexibility of cancer cells, which enables them to switch from using glycolysis to relying on mitochondrial metabolism (Ganapathy-Kanniappan and Geschwind, 2013; Sborov et al., 2015; Skoura et al., 2012). Conversely, it has been noted by our group and others that while utilizing mitochondrial metabolism, cancer cells demonstrate reduced sensitivity to chemotherapeutics and some targeted therapies (Haq et al., 2013; Park et al., 2016; Vazquez et al., 2013; Vellinga et al., 2015; Viale et al., 2014; Weinberg et al., 2010; Weinberg and Chandel, 2015). Thus, in addition to targeting glycolysis, optimal therapeutic exploitation of dysregulated metabolism in tumors will also require cancer-cell-selective inhibition of mitochondrial metabolism.

In order to survive periods of metabolic stress, cancer cells must be able to sense and respond to dramatic shifts in nutrient availability in their proximal environment. Mitochondria are a key component of such adaptive activities as they not only participate in the oxidation of glucose but can also oxidize fatty acids, glutamine, and lactate to satisfy the bioenergetic and/or biosynthetic needs of cancer cells (Faubert et al., 2017; Hui et al., 2017; Liu et al., 2016b; Park et al., 2016; Sonveaux et al., 2008; Wise et al., 2008). Not often considered in discussions of tumor metabolism is that the levels of glucose (and other nutrients) vary dramatically, both temporally and spatially, within tumors. Indeed, several studies have revealed that the intratumoral levels of glucose are less than 1 mM, implying that tumors are in a near constant state of glucose deprivation (Ho et al., 2015; Liu et al., 2016b). This puts into context our previous observation that when glucose is limiting, cancer cells can utilize lactate, an abundant carbon source within tumors (10–15 mM) and that its utilization requires the nuclear receptor ERRα (Park et al., 2016; Sonveaux et al., 2008). The importance of lactate was also highlighted by others in recent studies in non-small-cell lung cancers where lactate was shown to be the major fuel entering the tricarboxylic acid (TCA) cycle (Faubert et al., 2017; Hui et al., 2017). Indeed, blocking lactate uptake using small molecule inhibitors of the monocarboxylate transporter 1 (MCT1) is being considered as a therapeutic strategy in some cancers (Corbet et al., 2018; Sonveaux et al., 2008). These and other supporting studies suggest that reliance on lactate metabolism is a vulnerability of cancers and highlights the potential utility of ERRα as a therapeutic target.

Although the anti-cancer activities and the mechanism(s) of action of several small molecule inhibitors that target mitochondrial metabolism have been described, the efficacy of most of these agents are significantly impacted by fluctuations in nutrient and oxygen availability and by the inherent metabolic flexibility of cancer cells (e.g., metabolic shift between glycolysis and oxidative

This is an open access article under the CC BY-NC-ND license (http://creativecommons.org/licenses/by-nc-nd/4.0/).

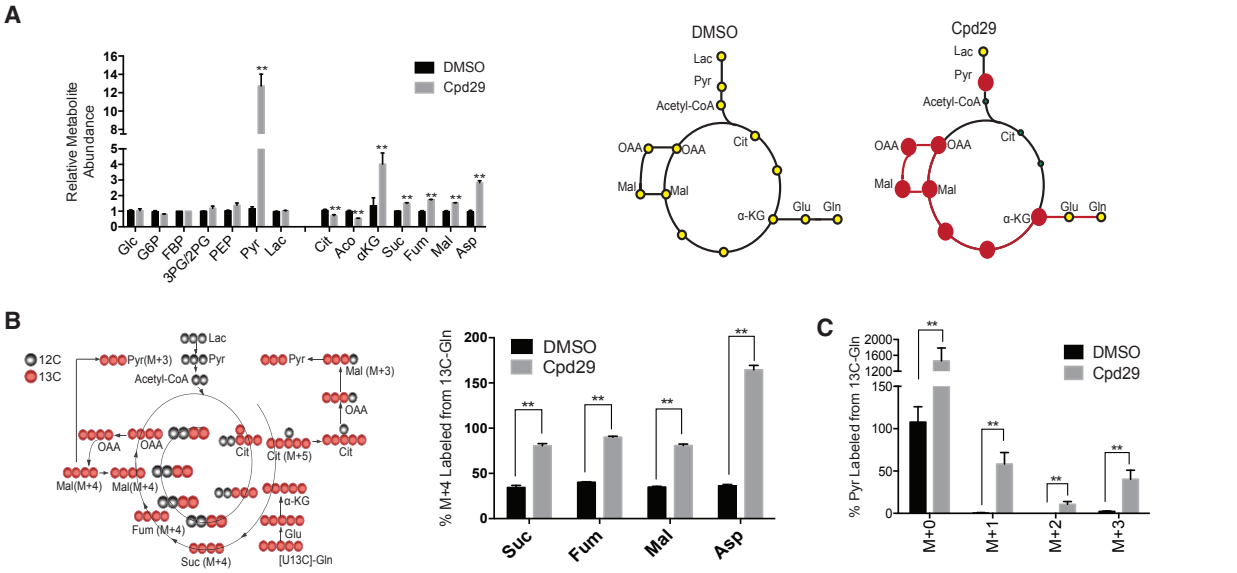

Figure 1. Metabolic Changes in Response to ERRα Inhibitor Cpd29 in Glucose-Deprived Conditions

(A) Relative abundance of indicated metabolites in MDA436 cells cultured in glucose and glutamine-free DMEM (10% dialyzed fetal bovine serum [FBS]) supplemented with 10 mM lactate + 2 mM glutamine (glucose-deprived conditions) and treated with DMSO or 5 μM Cpd29 for 24 h (left). A schematic representation of metabolic pathways upregulated in response to Cpd29. Red circles represent increased metabolites (right).

(B) A schematic representation of ^{13}C-glutamine incorporation into metabolites of the TCA cycle. Black and red circles are ^{12}C and ^{13}C, respectively (left). Percent of M+4 succinate, fumarate, malate, and aspartate in MDA436 cells following steady-state tracing (24-h labeling) with 10 mM lactate + 2 mM [U-^{13}C]-glutamine in the presence or absence of 5 μM Cpd29 (right).

(C) Mass isotopomer distribution of pyruvate in MDA436 cells grown in the same conditions as in (B). The levels of metabolites in Cpd29-treated group were normalized with respect to the relevant metabolites in DMSO controls.

The error bars represent SD (n = 3). The p value was calculated using two-tailed Student's t test, **$p < 0.05$. See also Figure S1.

phosphorylation [OXPHOS]) (Gui et al., 2016; Liu et al., 2016b; Muir and Vander Heiden, 2018; Park et al., 2016; Wolpaw and Dang, 2018). Blocking the activity of these compensatory pathways, together with the primary target, is a general approach that has been used to develop combinatorial interventions that inhibit cancer cell metabolism. Here, we have taken the alternative approach of identifying and exploiting conditional vulnerabilities that emerge in cells when treated with drugs directed against a specific metabolic pathway. We report the success of one such approach in which inhibition of the activity of the nuclear receptor ERRα inhibits pyruvate entry into mitochondria, with the result that cells become dependent upon glutamine and glucose oxidation to generate nicotinamide adenine dinucleotide phosphate (NADPH). In this manner, cancer cells are rendered hypersensitive to glutaminase (GLS1) inhibitors in conditions of low glucose availability and become acutely dependent on both glutamine (glutaminolysis) and glucose entry into the pentose phosphate pathways in glucose-replete conditions. Therapeutic exploitation of these induced vulnerabilities was shown to be an effective therapeutic strategy in clinically relevant animal models of breast cancer.

RESULTS

Inhibition of ERRα Increases Oxidative Glutamine Metabolism

Whereas cancer cells have a proclivity for glucose utilization, they are for the most part in a constant state of glucose deprivation as intratumoral levels of glucose rarely exceed 1 mM (Ho et al., 2015; Liu et al., 2016b). Cancer cells can survive glucose deprivation by switching to use lactate as their primary carbon source, an adaptive event that we have shown requires the nuclear receptor ERRα (Park et al., 2016). Specifically, it was demonstrated that lactate oxidation and incorporation of lactate-derived carbons into TCA cycle intermediates was decreased in ERRα antagonist Cpd29-treated cells (Park et al., 2016). Considering these data, we embarked on studies to define the mechanisms by which ERRα impacts lactate metabolism with the goal of identifying targetable vulnerabilities that were exposed in cells in which this particular activity of ERRα was inhibited.

As a first step, we performed metabolite profiling in MDA-MB-436 (MDA436) cells (a model of triple negative breast cancer [TNBC]) grown in 10 mM lactate + 2 mM glutamine (glucose-deprived conditions). This revealed a significant decrease of citrate and aconitate as would have been predicted from reduced lactate oxidation upon ERRα inhibition (Park et al., 2016). However, it was also observed that there was a concomitant accumulation of pyruvate, α-ketoglutarate, succinate, fumarate, malate, and aspartate in cells upon ERRα inhibition (Figure 1A). Given that lactate and glutamine are the major metabolic fuels in these culture conditions, it was speculated that the increased levels of α-ketoglutarate, succinate, fumarate, malate, and aspartate observed upon ERRα inhibition resulted from increased glutamine flux into the TCA cycle to compensate for decreases in

lactate oxidation. To test this hypothesis, MDA436 cells were propagated in the same glucose-deprived conditions with ^{13}C-glutamine (10 mM lactate + 2 mM [U-^{13}C] glutamine) for 24 h and the steady-state enrichment of isotope-labeled metabolites were assessed. It was observed that the abundance of fully labeled (M+4) succinate, fumarate, malate, and aspartate was significantly increased in Cpd29-treated cells, confirming that cells increased their reliance on glutamine anaplerosis when lactate flux into mitochondria was suppressed following ERRα inhibition (Figure 1B). Similar results were observed in studies performed in HCC1937 cells grown in glucose-deprived conditions (10 mM [U-^{13}C] lactate + 2 mM glutamine) with an accumulation of pyruvate and a reduction of incorporation of lactate carbon into citrate and aconitate noted in Cpd29-treated cells (Figures S1A–S1C). Glutamine incorporation (M+0 metabolites of glutamate, α-ketoglutarate, and aspartate) was also increased (Figure S1D). Examination of isotope enrichment of pyruvate in this study was particularly informative. The increase in M+3 pyruvate observed could result from oxidative and/or reductive pathways of glutamine utilization (Figures 1B and 1C). While reductive carboxylation of glutamine does occur in these glucose-deprived conditions, as evidenced by the presence of M+5 citrate from [U-^{13}C] glutamine, there is no significant difference in M+5 citrate in control versus ERRα-inhibited cells (Figure S1E). Thus, flux through this pathway is unlikely to account for the increased glutamine-derived pyruvate observed in Cpd29-treated cells (Figure 1C). In the oxidative glutaminolysis pathway, glutamine is oxidized in the mitochondria and can be converted to pyruvate via malic enzymes (MEs). It was previously shown that in glucose-deprived conditions, pyruvate can be generated from glutamine via mitochondrial ME (ME2) (Yang et al., 2014). However, the observed increase in M+3 pyruvate from [U-^{13}C] glutamine can also arise via cytosolic ME (ME1) where glutamine is oxidized to oxaloacetate (OAA) and exported from the mitochondria through the malate-aspartate shuttle and converted to malate by malate dehydrogenase 1 (MDH1) and then to pyruvate via cytosolic ME1. This latter pathway was found to be active and would be consistent with our previous studies indicating that the activity of the malate-aspartate shuttle is required for lactate utilization as knockdown of MDH1 expression compromised the ability of lactate to rescue cell viability (Park et al., 2016). Collectively, these results indicate that upon ERRα inhibition cancer cells limit the flux of lactate-derived pyruvate into mitochondria and increase their reliance on oxidative glutamine metabolism through the TCA cycle and the malate-aspartate shuttle.

ERRα Is Required for the Maintenance of NADPH

One consequence of inhibiting lactate oxidation in glucose-deprived conditions is that cancer cells are unable to use lactate-derived carbons to drive the production of NADPH, likely rendering cells dependent on glutamine for this activity. NADPH is a key cofactor required not only for biomass synthesis but also to maintain redox balance in cells (Fan et al., 2014; Liu et al., 2016a). One unit of NADPH is produced when malate is converted into pyruvate via MEs. NADPH produced in this manner can be used to reduce oxidized glutathione (GSSG) to reduced glutathione (GSH), which in turn is required to mitigate the impact of reactive oxygen species (ROS) (Figure 2A). We have previously shown that lactate-derived malate was decreased upon ERRα inhibition, which would likely result in a decrease in cellular NADPH levels, rendering cancer cells more susceptible to oxidative stress (Park et al., 2016). Therefore, we hypothesized that ERRα inhibition interferes with cellular redox balance, resulting in increased ROS production. In response, glutamine is rerouted to NADPH synthesis pathways to mitigate the impact of ROS on cell survival. The increased reliance on glutamine likely reflects the need to maintain redox balance, as opposed to generation of biomass, as cells are not proliferating in glucose-deprived conditions. To test this hypothesis, we assessed NADPH and ROS levels in MDA436 cells treated with or without an ERRα antagonist Cpd29. We observed a decrease in NADPH levels upon ERRα inhibition (Figure 2B), and this was associated with increased ROS production and apoptosis (Figures 2C and S2A). Importantly, all of these changes were prevented when cells were supplemented with 10 mM glutamine (Figures 2C and 2D). In parallel, cell proliferation assays were performed under the conditions where glutamine (2 mM) was maintained during the course of the experiment by replenishing it every 2 days. This continuous glutamine supplementation regimen protected against ERRα-antagonist-induced cell death (Figure 2E). Similarly, a one-time addition of 10 mM glutamine was found to prevent cell death induced by ERRα inhibition (both chemical inhibitor and small interfering RNA [siRNA]-mediated knockdown) (Figures 2F and 2G). However, addition of the GLS1 inhibitors BPTES or CB-839 compromised the ability of supplemental glutamine to rescue cell survival or to reduce ROS levels (Figures 2E and 2F; Figures S2B and S2C). Furthermore, supplementation of media with GSH abrogated the toxicity of ERRα and GLS1 inhibitors on cancer cell survival (Figures 2H and 2J) and reduced ROS levels (Figures 2I, S2B, and S2C). Similar results were also observed in HCC1937 cells (Figures S2D–S2G). These results confirmed that ROS is a contributing factor to cell death under glucose-deprived conditions and that ERRα is required to mitigate these activities.

Inhibition of ERRα Leads to a Compensatory Upregulation of Pathways That Are Involved in NADPH Synthesis

The results of studies described thus far indicate that ERRα is likely a useful therapeutic target in settings where glucose levels are limited. However, given the very dramatic fluctuations in intratumoral glucose levels (Trédan et al., 2007), it was important to determine whether the vulnerabilities exposed in glucose-deprived conditions upon ERRα inhibition were also present in glucose-replete conditions. Thus, metabolomic profiling experiments were performed under conditions of 12.5 mM glucose + 2 mM glutamine with or without ERRα inhibition. Surprisingly, as shown in Figure 3A, pyruvate, succinate, fumarate, malate, and aspartate also accumulated in these conditions upon Cpd29 treatment. To gain detailed insight into substrate utilization in ERRα-inhibited cells, we cultured MDA436 cells in media supplemented with [U-^{13}C] glucose or [U-^{13}C] glutamine for 24 h and analyzed steady-state isotope enrichment. In culture conditions with 12.5 mM glucose + 2 mM glutamine, (1) most of the total cellular pool of glycolytic intermediates were derived from

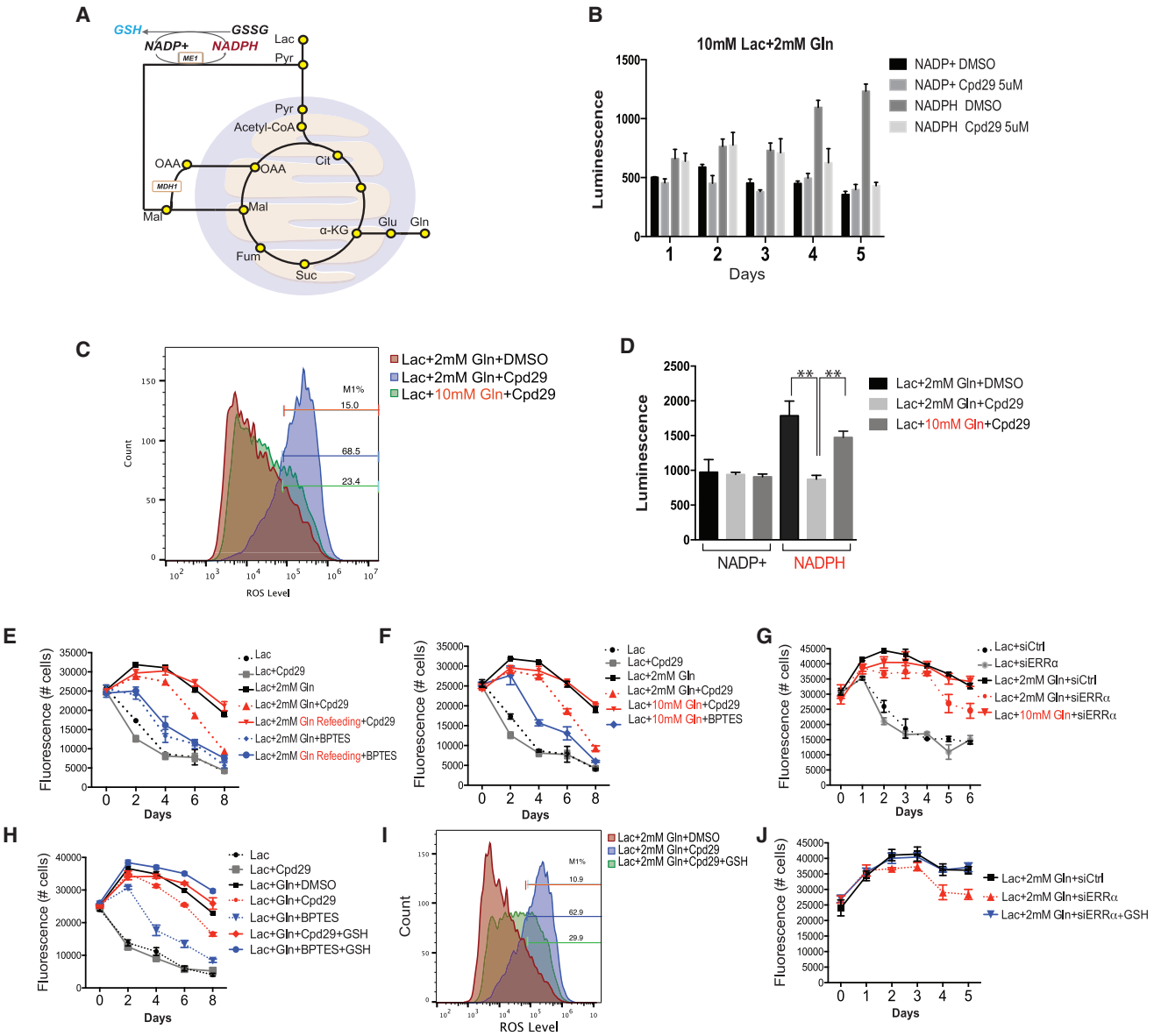

Figure 2. Upon ERRα Inhibition, Glutamine Flux into Mitochondria Is Increased to Generate NADPH

(A) A schematic representation of mitochondrial NADPH synthesis pathway.

(B) $NADP^+$ and NADPH levels were determined over time in MDA436 cells cultured in glucose and glutamine-free DMEM (10% dialyzed FBS) supplemented with 10 mM lactate + 2 mM glutamine in the treatment of DMSO or 5 μM Cpd29.

(C) MDA436 cells were incubated for 48 h in glucose and glutamine-free DMEM (10% dialyzed FBS) supplemented with 10 mM lactate + 2 mM glutamine or 10 mM lactate + 10 mM glutamine in the presence of Cpd29, and cells were then incubated with CM-H_2DCFDA for 60 min and the intensity of fluorescence was measured using flow cytometry.

(D) MDA436 cells were cultured for 3 days in the same conditions as in (C), and the levels of $NADP^+$ and NADPH were measured.

(E and F) MDA436 cells were cultured in the indicated media in the presence of Cpd29 or BPTES (1 μM) and harvested at the time points shown, and cell numbers were determined.

(G) MDA436 cells were transfected with control (siCtrl) or ERRα (siERRα) siRNAs for 48 h. Cells were then switched to the indicated media. Cells were harvested at the time points shown, and cell numbers were determined.

(H) MDA436 cells were cultured in the indicated media in the presence of GSH (10 mM), and cell numbers were determined.

(I) ROS levels were measured in the presence of indicated treatments for 48 h.

(J) MDA436 cells were transfected with control (siCtrl) or ERRα (siERRα) siRNAs for 48 h. Cells were then switched to the indicated media in the absence or presence of GSH. Cells were harvested at the time points shown, and cell numbers were determined. Cell numbers were determined by staining with the DNA dye Hoechst 33258.

The error bars represent SD (n = 3). The p value was calculated using two-tailed Student's t test, $^{**}p < 0.05$. See also Figure S2.

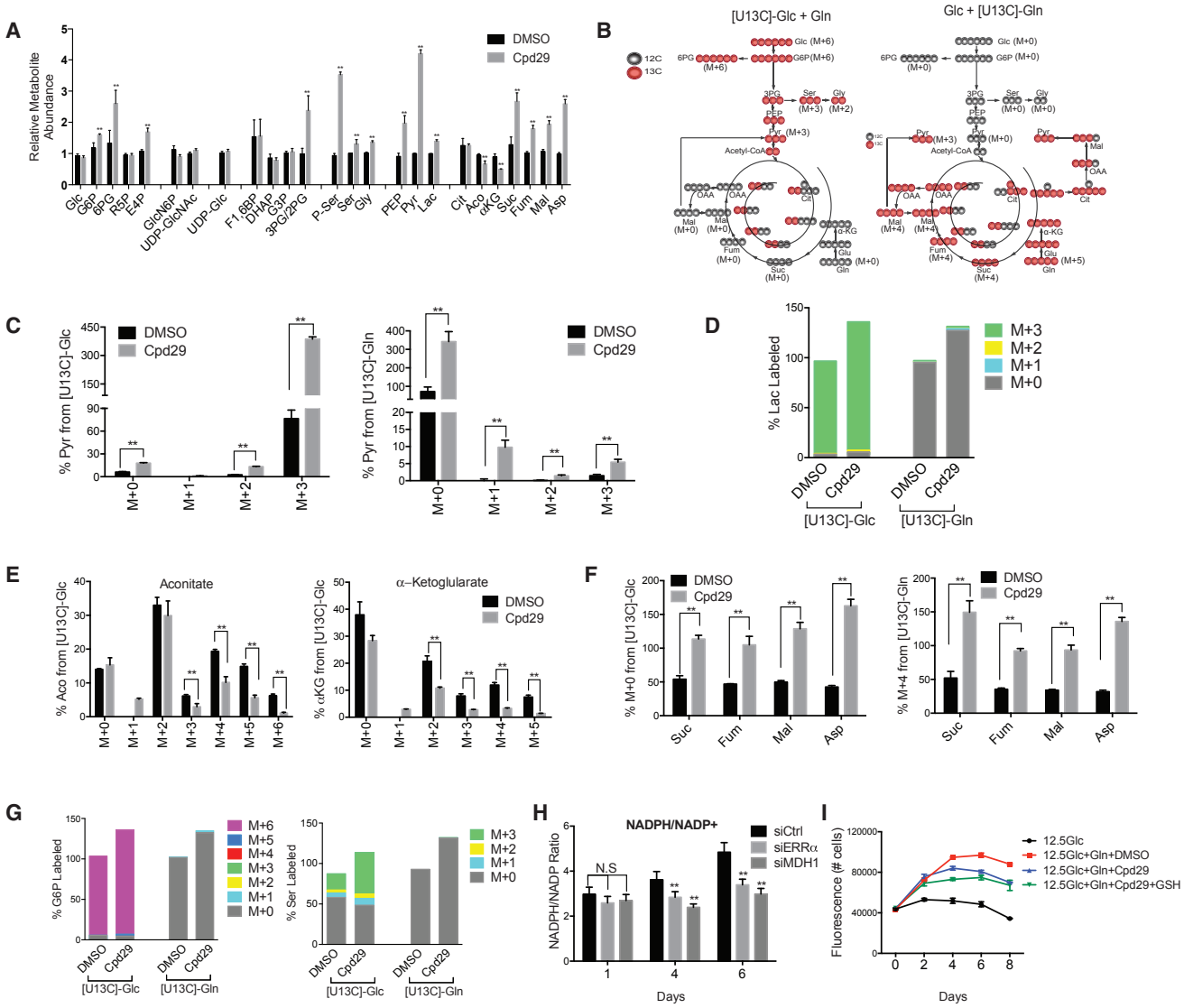

Figure 3. ERRα Inhibition Leads to a Compensatory Upregulation of Glucose Flux into Pentose Phosphate Pathway and OCM and Glutamine Flux into Mitochondria

(A) Relative abundance of indicated metabolites in MDA436 cells cultured in glucose and glutamine-free DMEM (10% dialyzed FBS) supplemented with 12.5 mM glucose + 2 mM glutamine in the treatment of DMSO or 5 μM Cpd29 for 24 h.

(B) A schematic representation of ^{13}C-glucose or ^{13}C-glutamine incorporation into metabolites. Black and red circles are ^{12}C and ^{13}C, respectively.

(C and D) Mass isotopomer distribution of pyruvate (C) and lactate (D) in MDA436 cells grown in glucose and glutamine-free DMEM (10% dialyzed FBS) supplemented with 12.5 mM [U-^{13}C] glucose + 2 mM glutamine or 12.5 mM glucose + 2 mM [U-^{13}C] glutamine in the presence of DMSO or Cpd29 for 24 h.

(E) Mass isotopomer distribution of aconitate and α-ketoglutarate from 12.5 mM [U-^{13}C] glucose + 2 mM glutamine in the presence of DMSO or Cpd29 for 24 h.

(F) Relative abundance of M+0 or M+4 succinate, fumarate, malate, and aspartate in MDA436 cells cultured in glucose-free media supplemented with 12.5 mM [U-^{13}C] glucose + 2 mM glutamine or 12.5 mM glucose + 2 mM [U-^{13}C] glutamine for 24 h in the presence or absence of 5 μM Cpd29.

(G) Mass isotopomer distribution of glucose-6-phosphate (G6P) and serine from cells cultured in 12.5 mM [U-^{13}C] glucose + 2 mM glutamine or 12.5 mM glucose + 2 mM [U-^{13}C] glutamine for 24 h in the presence or absence of 5 μM Cpd29. In all isotopomer analyses, the levels of metabolites in Cpd29-treated group were normalized with respect to the relevant metabolites in DMSO controls.

(H) MDA436 cells were transfected with control (siCtrl), ERRα (siERRα), or MDH1 (siMDH1) siRNAs in media with 12.5 mM glucose + 2 mM glutamine (glucose-replete media), and NADPH/NADP$^+$ ratio was determined.

(I) MDA436 cells were cultured in the indicated media in the presence of 10 mM GSH, and cell numbers were determined by staining with the DNA dye Hoechst 33258.

The error bars represent SD (n = 3). The p value was calculated using two-tailed Student's t test, $^{**}p < 0.05$. See also Figure S3.

glucose; (2) TCA cycle intermediates were derived from both glucose and glutamine; (3) alanine, serine, and glycine were derived from glucose; (4) proline, glutamate, and aspartate were made from both glucose and glutamine; (5) pyrimidines (UTP and CTP), derived from aspartate, were labeled with both ^{13}C-glucose and ^{13}C-glutamine, but purines (IMP, ATP, and AMP) were labeled predominantly with ^{13}C-glucose; and (6) only low amounts of the ^{13}C carbon were incorporated into fatty acids (Figure S3A). Stable isotope tracing experiments also revealed that upon ERRα inhibition, cells accumulate glucose-derived pyruvate, as evidenced by a marked enrichment of M+3 pyruvate from [U-^{13}C] glucose (and M+0 pyruvate from unlabeled glucose in [U-^{13}C] glutamine conditions), and significantly increased glutamine-derived pyruvate (enrichment of M+3 pyruvate from [U-^{13}C] glutamine and M+0 from unlabeled glutamine in [U-^{13}C] glucose conditions) was observed (Figures 3B and 3C). These data suggest that even under glucose-replete conditions, ERRα inhibition limits pyruvate entry into mitochondria, which may cause cells to have an increased reliance on oxidative glutamine metabolism. Decreased entry of glucose-derived pyruvate into mitochondria upon ERRα inhibition was further confirmed in studies that showed that the levels of ^{13}C-glucose-labeled aconitate and α-ketoglutarate were significantly reduced in response to Cpd29 treatment (Figure 3E). However, one difference in carbon fate noted was that the reductive carboxylation of glutamine was found to be different from that observed in glucose-deprived conditions. As described above, reductive carboxylation of glutamine was not affected by Cpd29 in glucose-deprived conditions. However, M+5 citrate enrichment was significantly increased in glucose-replete conditions in response to Cpd29 (Figure S3B). More detailed tracing experiments revealed that upon ERRα inhibition, the abundance of fully labeled (M+4) succinate, fumarate, malate, and aspartate, derived from ^{13}C-glutamine, was significantly increased in Cpd29-treated cells, highlighting their reliance on glutamine anaplerosis (Figure 3F). In previous studies, we showed that the decrease in oxygen consumption rate observed upon ERRα inhibition was accompanied by an increase in the extracellular acidification rate, indicative of increased lactate production (Park et al., 2016; Yuk et al., 2015). This was likely due to increased glycolysis as treatment of cells with the ERRα antagonist Cpd29 also resulted in increased glucose consumption and an increase in lactate production when cells were grown in glucose-replete conditions. Consistent with this observation, our metabolomic profiling analysis confirmed that lactate production from glucose was increased in response to ERRα inhibition (Figure 3D). This study further revealed that glucose flux into the pentose phosphate pathway (PPP) and one-carbon metabolism (OCM) pathways were increased in response to Cpd29 with no changes noted in the hexosamine and glycogenesis pathways (Figure 3A). Specifically, the levels of ^{13}C-glucose-derived M+6 isotopologs of glucose-6-phosphate (G6P) and 6-phosphogluconate (6PG) and M+0 derivatives of these isotopologs in ^{13}C-glutamine-labeled condition were increased in Cpd29-treated cells, findings that are consistent with increased entry of glucose carbon into the PPP pathway (Figures 3G and S3C). Further, the increase in serine (M+3) and glycine (M+2) in cells labeled with ^{13}C-glucose observed was indicative of increased flux of glucose into the OCM pathways (Figures 3G and S3D). Collectively, these findings indicate that ERRα inhibition resulted in an increased flux of glutamine into the mitochondria and increased glucose flux into the NADPH generating PPP and OCM pathways. Thus, even under glucose-replete conditions, ERRα inhibition may result in a disruption of NADPH homeostasis by uncoupling glycolysis and oxidative metabolism, forcing cells to upregulate the OCM and PPP pathways to maintain cellular NADPH levels. Indeed, in glucose-replete conditions, ERRα inhibition also decreased NADPH levels and induced apoptosis at later time points in glucose-replete conditions (Figures 3H and S3E). Consistent with the observation that cells require a functional malate-aspartate shuttle in glucose-deprived conditions, MDH1 knockdown also significantly reduced NADPH levels in glucose-replete conditions (Figure 3H). However, the growth inhibitory phenotype observed upon ERRα inhibition in glucose-replete conditions is not likely due to a failure to maintain GSH as its supplementation did not rescue the toxicity associated with ERRα inhibition (Figure 3I). Given the important role of NADPH in biomass synthesis, the reduction of NADPH in ERRα-inhibited cells in these conditions might be causally associated with the defect in supporting biomass synthesis.

ERRα Controls Pyruvate Flux into Mitochondria by Regulating the Expression of the MPC

The accumulation of pyruvate observed upon ERRα inhibition in both glucose-deprived and -replete conditions could result from decreased pyruvate transport into mitochondria. Pyruvate transport across the inner mitochondrial membrane is accomplished by a recently identified protein complex composed of mitochondrial pyruvate carrier (MPC) 1 and 2 that together facilitate pyruvate transport (Bricker et al., 2012; Herzig et al., 2012; Schell et al., 2014; Vacanti et al., 2014; Yang et al., 2014). To investigate whether the reduction of pyruvate transport into mitochondria observed upon ERRα inhibition is a consequence of downregulated MPC1 expression, we assessed the mRNA and protein levels of MPC1 upon ERRα inhibition. Inhibition of ERRα with siRNA or the ERRα antagonist Cpd29 significantly downregulated mRNA and protein expression of MPC1 in both MDA436 and HCC1937 cells (Figures 4A and 4B; Figures S4A–S4D). Inhibition of ERRα modestly decreased both total PDH and phosphorylated PDH levels, which was somewhat expected because PDH is also a known ERRα target gene. However, no effect on the abundance of mitochondrial protein VDAC was observed (Figures 4A and 4B). Based on these data, we next sought to assess the role of ERRα in MPC1 regulation at the transcriptional level in more detail. Although small molecule agonists for ERRα have not yet been identified, we have previously demonstrated that the activity of ERRα can be regulated by manipulating the expression level of its obligate coregulator PGC1α (Gaillard et al., 2006). As shown in Figures 4C and 4D, expression of PGC1α or PGC1α_2X9 (a PGC1α derivative engineered to be highly selective for ERRα) dramatically induced both MPC1 mRNA and protein expression, whereas PGC1α_L2L3M (engineered PGC1α unable to bind to ERRα) was without activity in this assay. Two different siRNAs against ERRα were used to demonstrate that ERRα was required for the expression of

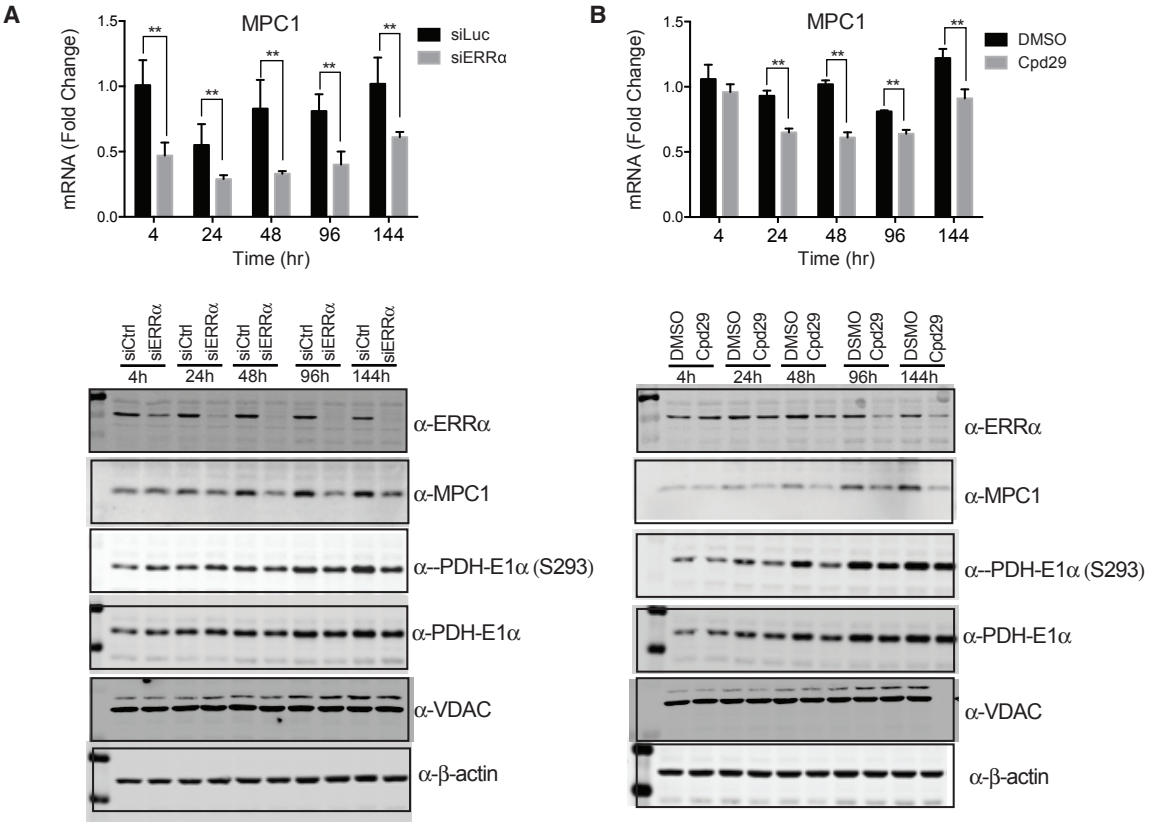

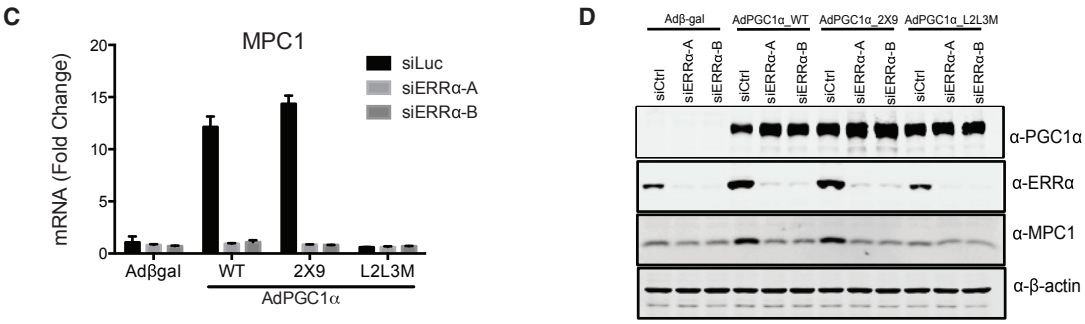

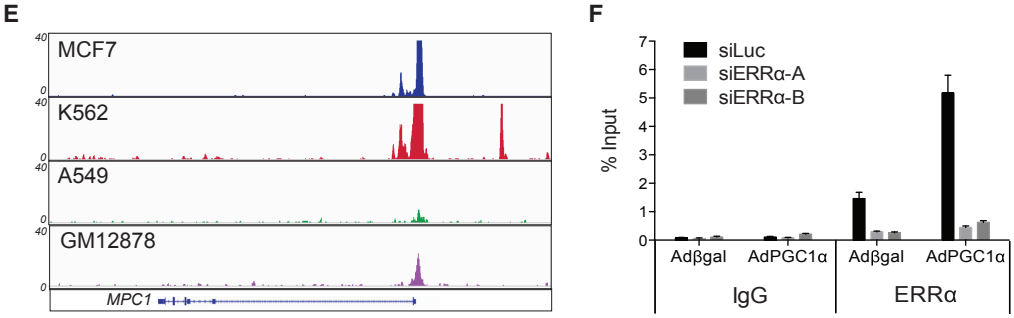

(legend on next page)

MPC1 in the PGC1α expressing cells. In order to explore whether ERRα directly regulates the expression of MPCs, we searched for ERRα occupancy within the MPC1 locus in publicly available chromatin immunoprecipitation sequencing (ChIP-seq) datasets (ENCODE) for which genome-wide ERRα binding profile data was available for several cell lines, including MCF7, A549, GM12878, and K562. This revealed significant enrichment of ERRα occupancy on the MPC1 promoter (Figure 4E). Next, we performed a ChIP assay using PCR primers against the enriched genomic regions retrieved from the ENCODE database to examine whether ERRα is directly recruited to the MPC1 promoter in MDA436 cells (Figure 4E). In this manner, it was determined that ERRα is directly recruited to the MPC1 promoter, confirming that it is a direct transcriptional target gene of this receptor (Figure 4F).

MPC1 Overexpression Restores Pyruvate Flux into Mitochondria in ERRα-Inhibited Cells

In light of the observation that ERRα inhibition downregulates MPC1 expression, we employed an overexpression system, wherein MPC1 expression was placed under the control of a constitutive promoter, to test the necessity of MPC1 downregulation for the metabolic phenotype of ERRα-inhibited cells. As the functional MPC complex consists of an obligate heterodimer of MPC1 and MPC2 (Schell et al., 2014), we coexpressed both components using lentiviruses for these studies (Figure 5A). The effects of MPC1/2 overexpression in ERRα-inhibited cells was assessed by metabolite profiling in MDA436 cells grown in glucose-deprived conditions (10 mM lactate + 2 mM glutamine). This revealed that the increase in pyruvate accumulation observed upon ERRα inhibition was abrogated by MPC1/2 overexpression (Figure 5B). Isotope tracing experiments further confirmed that pyruvate accumulation (M+3 pyruvate from ^{13}C-lactate) observed upon Cpd29 treatment was almost reversed by MPC1/2 overexpression and that pyruvate oxidation was resumed, as evidenced by increased labeling of ^{13}C-lactate-derived carbons into citrate and aconitate in MPC1/2 overexpressing cells even in the presence of Cpd29 (Figures 5C and 5D). We next asked whether the effect of ERRα inhibition on cancer cell proliferation could be reversed with MPC1 overexpression. Indeed, MPC1/2 overexpression prevented cell death caused by ERRα inhibition when pyruvate was used as the sole substrate (Figure S5). Similarly, when either lactate or glucose was used as a carbon substrate, cell death caused by ERRα inhibition was also prevented by MPC1/2 overexpression (Figures 5E and 5F). Further, we also observed that the MPC inhibitor UK5099 functioned in a similar manner as the ERRα antagonist in assays of cell proliferation (Figures 5G and S5). These data show that MPC1/2 overexpression restores pyruvate flux into mitochondria in ERRα-inhibited cells and that this protects cells against ERRα-antagonist-induced cell death.

Co-inhibition of ERRα and NADPH Homeostatic Pathways as a Therapeutic Approach in Cancer

Our comprehensive metabolite profiling and stable isotope tracing studies enabled the generation of a "metabolic signature" that reports on ERRα activity in cancer cells. These data have informed the rational design of combination therapies that incorporate the concurrent targeting of ERRα together with additional vulnerabilities introduced into cells upon ERRα inhibition. Specifically, our data indicate that breast cancer cells treated with the ERRα antagonist Cpd29 were forced to upregulate glutamine flux into mitochondria and glucose flux into PPP and one-carbon metabolic pathways to compensate for the loss of NADPH (Figure 6A), and this creates targetable vulnerabilities. Thus, combinations of ERRα antagonists, with drugs targeting key enzymes in these compensatory pathways—GLS1 in glutaminolysis, glucose-6-phosphate dehydrogenase (G6PD) in PPP or dihydrofolate reductase (DHFR) in the one-carbon pathways—were evaluated for efficacy in cellular models of breast cancer. Small molecule inhibitors of GLS1 (CB-839 or BPTES), G6PD (dehydroepiandrosterone [DHEA]), and DHRF (methotrexate [MTX]) have been developed. As shown in Figures 6B, S6A, and S6B, all combinations of these drugs were much more efficacious as inhibitors of MDA436 cell proliferation than single agents, and the efficacy of triple combinations was superior to double drug combinations. Similar results were found when these combinations were assessed in other TNBC cell lines (BT20, HCC1143, HCC1937, MDAMB231, BT549, and HCC1806) (Figures S6, S7A, and S7B). Although PPP and one-carbon metabolic pathways contribute to NADPH synthesis, they also play a critical role in nucleotide synthesis by providing glucose-derived 5-carbon sugars and purine/pyrimidine moieties. To determine the extent to which the inhibitory effect of DHEA and MTX can be attributed to nucleotide synthesis, we evaluated the ability of deoxynucleotide triphosphates (dNTPs), a source of both 5-carbon ribose ring and bases, to rescue the cytotoxic effect(s) of these drugs. In this manner, it was demonstrated that supplementation of media with dNTPs was able to rescue MTX-mediated cytotoxicity but not that observed upon DHEA treatment (Figure 6C). This indicates that the cytotoxicity of MTX in this model system is mainly due to deficiencies in DNA/RNA synthesis rather than changes in NADPH homeostasis. Follow-up studies with this drug were not undertaken.

Figure 4. MPC1 Is a Direct Transcriptional Target of ERRα

(A and B) MDA436 cells were transfected with control (siCtrl) or ERRα (siERRα) siRNAs (A) or treated with DMSO or Cpd29 (B) in glucose-replete media. RNA and protein were harvested over time, and the expression of MPC1 was analyzed by qRT-PCR and immunoblotting.

(C and D) MDA436 cells were transfected with either control (siCtrl) or ERRα (siERRα-A and siERRα-B) siRNAs for 24 h, followed by infection of adenoviruses expressing β-gal (negative control), wild-type PGC-1α, ERRα-selective PGC-1α (2X9), or the nuclear-receptor-binding-deficient PGC-1α (L2L3M) for 48 h. RNA (C) and protein (D) were harvested, and the expression of MPC1 was analyzed by qRT-PCR and immunoblotting.

(E) Tracks are retrieved from ENCODE ChIP-seq datasets and shown for MPC1 genomic regions with ERRα occupancy.

(F) ChIP was performed to validate ERRα recruitment to MPC1 genomic regions in MDA436 cells transfected with either control (siCtrl) or ERRα (siERRα-A and siERRα-B) siRNAs for 24 h, followed by infection of adenoviruses expressing β-gal (negative control), wild-type PGC-1α, ERRα-selective PGC-1α (2X9), or the nuclear-receptor-binding-deficient PGC-1α (L2L3M) for 48 h.

The error bars represent SD (n = 3). The p value was calculated using two-tailed Student's t test, $^{**}p < 0.05$. See also Figure S4.

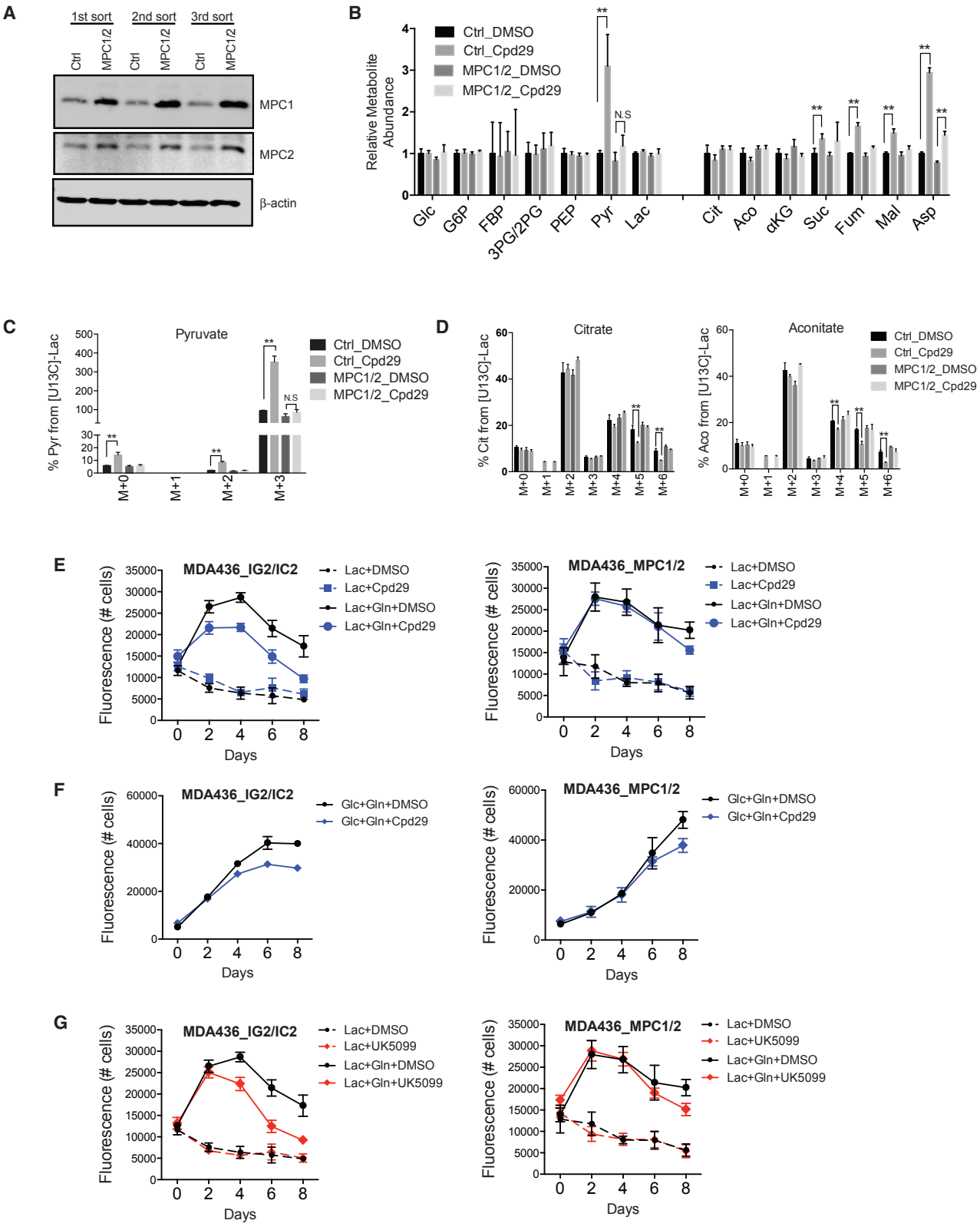

(legend on next page)

Increased Antitumor Activity by Combining an ERRα Antagonist with the GLS1 Inhibitor CB-839

The data presented thus far provide a strong rationale for the development of ERRα antagonists for use in combination with inhibitors of G6PD or GLS1 for the treatment of TNBC and possibly other cancers. Many cancers, TNBC among them, have been shown to be addicted to glutamine for their growth and metastasis, an observation that has highlighted the potential clinical utility of GLS1 as a therapeutic target (Gross et al., 2014; Xiang et al., 2015). Among the most developed compounds is the orally bioavailable GLS1 inhibitor CB-839, which has shown promise in both preclinical and clinical studies in multiple tumor types (Gross et al., 2014). Although safety and tolerability of CB-839 were the primary endpoints of a phase 1 clinical trial, preliminary efficacy as a single agent was limited to achieve long-term stable disease. However, CB-839 has been shown to be more effective when used in combination with other agents (E. Emberley et al., 2017, Keystone Symp., conference). With these encouraging data, the U.S. Food and Drug Administration (FDA) recently granted fast track designation to CB-839 in combination with cabozantinib or everolimus for the treatment of metastatic renal cancer patients (Tannir et al., 2018, Genitourin. Cancers Symp., abstract). Use of CB-839 in combination with other standard of care agents is currently being evaluated in phase 2 clinical trials in multiple tumor types. In this regard, our *in vitro* data strongly suggest that ERRα antagonists would likely improve the efficacy of GLS1 inhibitors. Therefore, we evaluated the potential clinical utility of these combinations using *in vivo* xenograft studies. Specifically, the efficacy of CB-839 (400 mg/kg/d) and DHEA (250 mg/kg/d) alone or in combination with Cpd29 (30 mg/kg/d) on the growth of MDA436 xenografts was assessed. The doses of Cpd29 and CB-839 used in this study did not cause any noticeable treatment-related toxicities (Figure 7B). DHEA was well tolerated and did not cause significant body-weight loss when used as a single agent (Figure S8). Unfortunately, its use was associated with significant morbidity and mortality in mice when combined with Cpd29 and therefore unsuitable for further exploration. As DHEA has many targets in addition to G6PD, therefore, more selective G6PD inhibitors are needed to explore the efficacy of triple combinations that include ERRα/GLS1 inhibitors. One of the most impactful findings of this study was that the combination of CB-839 and Cpd29 was significantly more effective than either therapy alone (Figure 7A). In sum, these studies suggest possible near-term clinical trials to test the utility of this multiple-pathway approach for targeting TNBC and other cancers.

DISCUSSION

Many oncogenic mutations rewire metabolism to enable maximal glucose utilization to support the biosynthetic and energetic needs of rapidly dividing cancer cells (Wolpaw and Dang, 2018). Not surprisingly, therefore, there has been a significant amount of interest in developing therapeutic strategies that target aerobic glycolysis. However, the efficacy of currently available interventions that target this pathway has been modest, an outcome that has been attributed, in part, to drug-induced compensatory events that increase cellular reliance on mitochondrial metabolism (Haq et al., 2013; Park et al., 2016; Vellinga et al., 2015; Viale et al., 2014). There is now a significant body of work indicating that in addition to ATP generation, mitochondria are involved in biomass generation, nucleotide synthesis, and the maintenance of redox balance, all of which are essential for the proliferation and survival of cancer cells (Bell et al., 2007; Birsoy et al., 2015; Di Lisa and Ziegler, 2001; Liu et al., 2016b; Pagliarini and Rutter, 2013; Stein and Imai, 2012; Sullivan et al., 2015). Cumulatively, these findings have driven the search for small molecules that can target mitochondrial metabolism in a cancer-cell-selective manner. In this regard, there is considerable interest of late in the potential anticancer activities of the electron transport chain (ETC) inhibitors metformin (complex I inhibitor), atovaquone (complex III inhibitor), and arsenic trioxide (complex IV inhibitor) (Ashton et al., 2018; Urra et al., 2017). There are a large number of on-going clinical trials assessing the efficacy of this class of drugs as cancer therapeutics.

Oxidation of lactate, glutamine, branched-chain amino acids, and fatty acids as occurs in tumors requires functional mitochondria. Lactate, for instance, is the most abundant carbon source in the tumor microenvironment and has long been considered a waste product of glycolysis. However, a number of recent studies have demonstrated that lactate is a major carbon source for cancer cells (Faubert et al., 2017; Hui et al., 2017; Park et al., 2016; Sonveaux et al., 2008). To serve as a fuel, lactate is first imported into cells, converted into pyruvate, and then crosses the mitochondrial matrix through the recently identified MPCs where it is oxidized (Bricker et al., 2012; Herzig et al., 2012). These important steps in lactate utilization have proved to be targetable and inhibitors of (1) MCT1, which mediates the import of lactate from the extracellular environment, and (2) MPCs, which facilitate pyruvate transport across the inner mitochondrial membrane, have been identified, and are under development. We have previously demonstrated that inhibition of nuclear receptor

Figure 5. MPC1 Overexpression Restores Pyruvate Flux into Mitochondria in ERRα-Inhibited Cells

(A) Western blot analysis of MDA436 cell lines with transduction of lentiviral targeting vector (Ctrl) or MPC1/2. MPC1/2 overexpressing cell lines were generated by fluorescence sorting three times.

(B) Relative abundance of indicated metabolites in control (Ctrl) and MPC1/2-expressing MDA436 cells cultured in glucose and glutamine-free DMEM (10% dialyzed FBS) supplemented with 10 mM lactate + 2 mM glutamine in the treatment of DMSO or 5 μM Cpd29 for 24 h.

(C and D) Mass isotopomer distribution of pyruvate (C), citrate, and aconitate (D) in Ctrl and MPC1/2-expressing MDA436 cells grown in glucose and glutamine-free DMEM (10% dialyzed FBS) supplemented with 10 mM [U-^{13}C] lactate + 2 mM glutamine in the presence of DMSO or Cpd29 for 24 h. The levels of metabolites were normalized with respect to the relevant metabolites in Ctrl-DMSO.

(E–G) Control (MDA436_IG2/IC2) and MPC1/2-expressing (MDA436_MPC1/2) cells were cultured in glucose-deprived (E) or glucose-replete media (F) in the presence of Cpd29 or MPC inhibitor UK5099 (5 μM) (G) and harvested at the time points shown, and cell numbers were determined. Cell numbers were determined by staining with the DNA dye Hoechst 33258.

The error bars represent SD (n = 3). The p value was calculated using two-tailed Student's t test, $^{**}p < 0.05$. See also Figure S5.

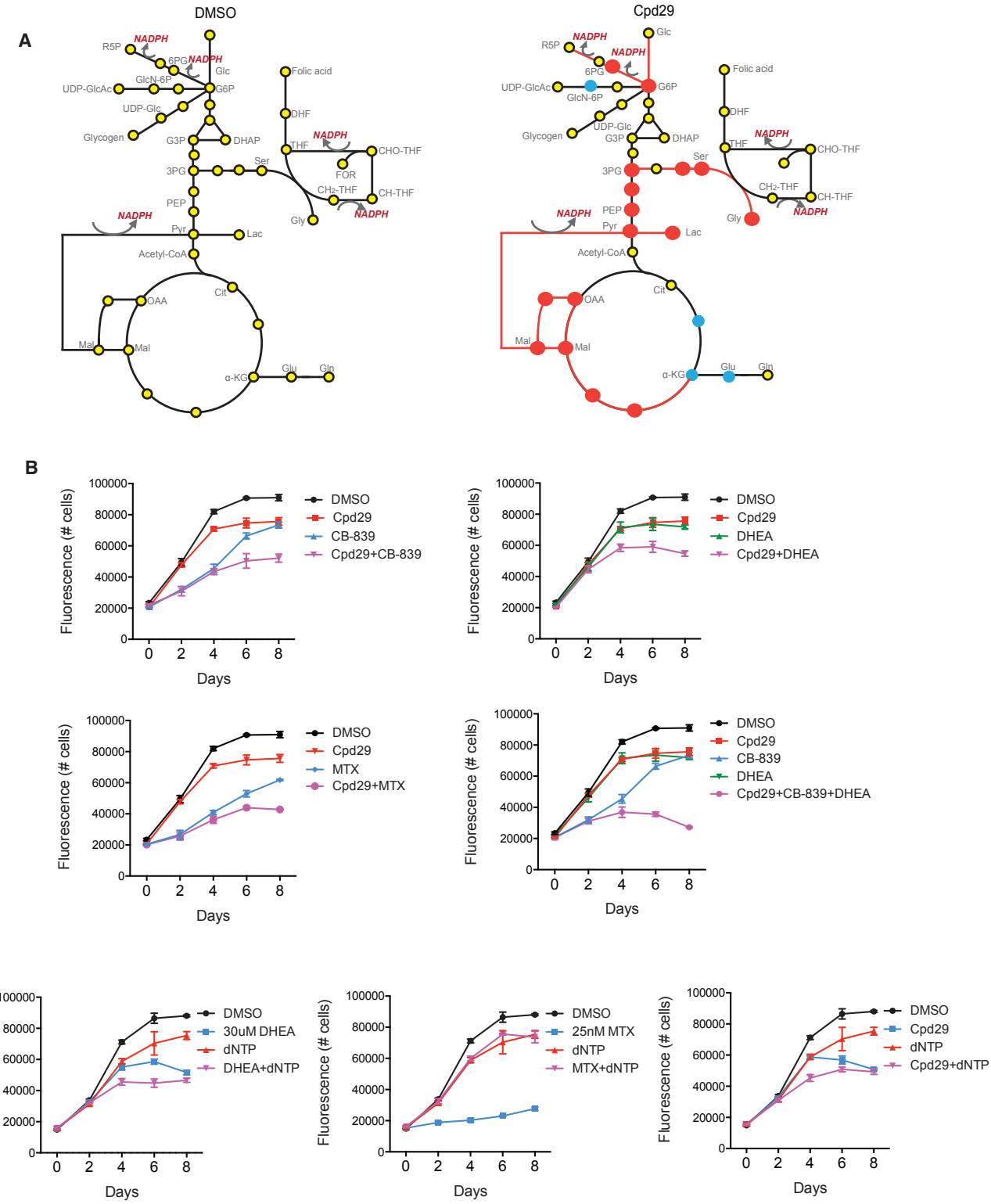

Figure 6. Cpd29 in Combination with Inhibitors Targeting NADPH Synthesis Pathways Is More Effective to Suppress Breast Cancer Cell Proliferation *In Vitro*

(A) A schematic representation of metabolite changes in response to Cpd29 in glucose-replete conditions. Red circle represents increased metabolites, and blue circle represents decreased metabolites.

(legend continued on next page)

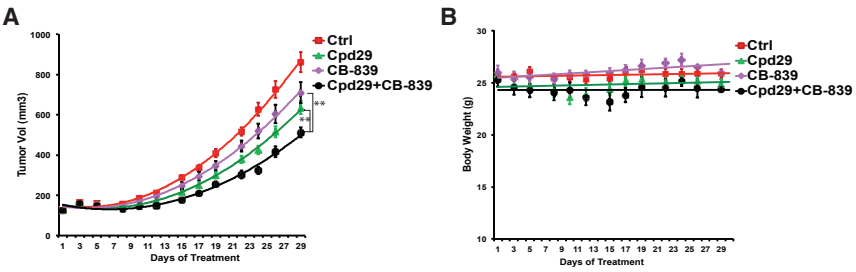

Figure 7. Analysis of ERRα Antagonist and CB-839 Combinations in an Animal Model of Breast Cancer

(A) MDA436 xenografts were treated with Cpd29 (30 mg/kg/day), CB-839 (400 mg/kg/day), or the combination of the two drugs and tumor volumes were measured throughout the experiment.

(B) Body weight was also monitored during the course of the experiment. Data are the mean of tumor volumes in each experimental group (Ctrl, n = 15; Cpd29, n = 14; CB-839, n = 9; Cpd29+CB-839, n = 8).

Error bars represent SEM. Statistical significance from single agent alone. The p value was calculated using two-way ANOVA followed by a Bonferroni multiple comparison test, **$p < 0.05$. See also Figure S7.

ERRα, genetically or using small molecule inhibitors, disrupts mitochondrial metabolism, impairs lactate utilization, and inhibits tumor growth in animal models of breast cancer. It is significant in this regard that we have determined that ERRα inhibition prevents the entry of lactate-derived pyruvate into mitochondria and directly and indirectly interferes with NADPH homeostasis. Whereas any inhibitor of mitochondrial function would likely impair lactate utilization, ERRα is particularly attractive as a target as its expression is generally very low in normal somatic cells and dramatically upregulated in transformed cells. Further, the very subtle phenotypes observed in ERRα knockout mice and the data showing that mice tolerate small molecule inhibitors of ERRα exceptionally well highlight the utility of using this class of inhibitors to effect a cancer-cell-selective inhibition of mitochondrial function.

ERRα has long been recognized as a master regulator of mitochondrial metabolism (Eichner and Giguère, 2011). This was further supported by ChIP-on-chip studies that showed that ERRα occupies the promoter regions of almost all the genes participating in the TCA cycle and OXPHOS (Charest-Marcotte et al., 2010; Eichner and Giguère, 2011). Although PGC1/ERRα increases expression of mRNA encoding proteins involved in mitochondrial metabolism, little to no work has been done to examine the impact of ERRα inhibition on the functionality of those genes. We have shown, using stable isotope tracers, how ERRα regulates the fate of lactate and glucose in cancer cells (Park et al., 2016). In the present study, we show that ERRα inhibition downregulates MPC1 and that this impairs pyruvate transport into mitochondria, resulting in cytosolic pyruvate accumulation. Considering the role of ERRα regulating the expression of genes encoding cell cycle, it was surprising that MPC1/2 expression alone was almost sufficient to rescue the metabolic and decreased cell proliferation phenotypes associated with ERRα inhibition. It is possible that MPC is the primary "gatekeeping" regulator of carbon entry into TCA cycle, and thus its downregulation results in a bottleneck at the entrance to the TCA cycle. It is also possible that the impact of downregulating the expression of other TCA cycle genes is relatively minor and can be mitigated by increased expression of MPC. Regardless, we conclude that the ability of ERRα inhibitors to decrease MPC1 expression is an essential component of their anti-tumor efficacy.

One of the problems with existing strategies used to target metabolism in cancer is that most cells have the ability to rewire their metabolism to survive the primary pharmaceutical insult. This has led to the development of strategies to target both primary and escape pathways. Considering its cancer-cell-selective overexpression and the availability of small molecule inhibitors, ERRα is a particularly attractive co-target for such regimens. Using ERRα inhibition as a base upon which to build new therapeutic strategies, we screened for pathways that were induced upon the inhibition of the activity of this nuclear receptor. Among the most interesting vulnerabilities observed was the increased reliance of cells on glutamine to restore NADPH homeostasis. The significance of this observation was confirmed in tumor models where it was shown that the efficacy of a clinically important GLS1 inhibitor was significantly increased in ERRα-inhibitor-treated animals. Indeed, near-term testing of ERRα inhibitors, in combination with existing GLS1 inhibitors, is certainly justified by these findings. Our studies also highlight the potential utility of adding G6PD inhibitors to ERRα antagonist and GLS1 inhibitor combinations. However, the toxicity in animals of combining DHEA and ERRα antagonists limited our ability to test this particular combination. It is unclear why ERRα inhibition predisposes animals to DHEA toxicity, although the mechanisms underlying this activity are currently under investigation as is a search for additional pathways that can be co-targeted with ERRα in tumors.

One of the most attractive features of ERRα antagonists is that they exploit the fact that this receptor is significantly overexpressed in cancers and thus affords the opportunity to target cancer cell mitochondrial function in a selective manner. In addition to increasing the efficacy of agents that target different aspects of mitochondrial metabolism, our studies also suggest alternative uses for ERRα antagonists in cancer. Of late there has been considerable interest in exploiting ETC inhibitors in

(B) MDA436 cells were treated with ERRα antagonist Cpd29 (5 μM), GLS1 inhibitor CB-839 (1 μM), G6PD inhibitor DHEA (30 μM), or DHFR inhibitor MTX (25 nM) alone or in combination for 8 days. Cell numbers were determined by staining with Hoechst 33258.

(C) MDA436 cells were cultured in glucose-replete media with the indicated pharmacological inhibitors in the presence or absence of dNTP mix (100 μM each). Cells were harvested at the time points shown, and cell numbers were determined by staining with the DNA dye Hoechst 33258.

See also Figure S6.

combination with radiation therapy in solid tumors (Cheng et al., 2016; Jordan and Sonveaux, 2012). The rationale underlying this strategy is that the reduced oxygen consumption in response to ETC inhibitors may alleviate tumor hypoxia and tumor hypoxia has been shown to be associated with a poor response to radiotherapy in many types of tumors (Dhani et al., 2015; Gilkes et al., 2014). Inhibitors of ETC reduce OCR (oxygen consumption rate) and result in an increase in oxygen availability within tumors (Ashton et al., 2016; Diepart et al., 2012; Jordan and Sonveaux, 2012; Zannella et al., 2013). A novel complex I inhibitor, BAY87-2243, was shown to alleviate hypoxia and improve radiation response in preclinical models, however, a phase I clinical trial with this drug had to be terminated due to unexpected toxicity (Chang et al., 2015; Ellinghaus et al., 2013). As previously shown, inhibition of ERRα also reduces OCR in breast cancer cells (Luo et al., 2017; Park et al., 2016). This might reflect the fact that many of the nuclear-encoded ETC genes are direct transcriptional targets of ERRα (Chang et al., 2011; Charest-Marcotte et al., 2010; Luo et al., 2017). Regardless, considering the mechanism of action of ERRα, and the apparent safety of inhibitors of this receptor, it is likely that drugs of this class would also function as radiosensitizers.

Our studies have highlighted a central role for ERRα in regulating the adaptive processes used by tumors to thrive in conditions of fluctuating nutrient availability. This, combined with the fact that it is a druggable transcription factor, make it an extremely attractive therapeutic target, the exploitation of which is likely to have a significant impact on the pharmacotherapy of multiple tumor types.

STAR★METHODS

Detailed methods are provided in the online version of this paper and include the following:

- KEY RESOURCES TABLE
- CONTACT FOR REAGENT AND RESOURCE SHARING
- EXPERIMENTAL MODELS AND SUBJECT DETAILS
  - Animals and In Vivo Procedures
  - Cell Culture
- METHOD DETAILS
  - Proliferation Assay
  - U-^{13}C Glutamine and U-^{13}C Glucose Isotopomer Analysis
  - LC-MS Analysis
  - Quantitative PCR
  - Western Blot Analysis
  - Chromatin Immunoprecipitation Assay (ChIP)
  - Adenoviral Transduction
  - NADP$^+$ and NADPH measurement
  - ROS Generation Assay
  - Apoptosis Assay
- QUANTIFICATION AND STATISTICAL ANALYSIS

SUPPLEMENTAL INFORMATION

Supplemental Information can be found online at https://doi.org/10.1016/j.celrep.2019.05.066.

ACKNOWLEDGMENTS

We thank Dr. Jared Rutter for kindly providing the MPC1 and MPC2 expressing lentiviral vectors and Dr. Christopher Newgard and members of the McDonnell lab for the useful discussion and advice. This work was supported by NIH R01CA174643 (D.P.M.), UL1TR001117 (D.P.M.), R00CA168997 (J.W.L.), and R01CA193256 (J.W.L.) and a Susan G. Komen Fellowship PDF12227913 (S.P.).

AUTHOR CONTRIBUTIONS

S.P., C.-Y.C., J.W.L., and D.P.M. designed the experiments. R.S. designed and analyzed ROS and apoptosis assay. X.L. and J.L designed and performed metabolomics. R.B. and W.L. designed and performed the animal experiments. S.P. performed, analyzed, and interpreted the majority of the experiments. S.P. and D.P.M. wrote the manuscript with input from all authors.

DECLARATION OF INTERESTS

The authors declare no competing interest.

Received: August 30, 2018
Revised: April 3, 2019
Accepted: May 17, 2019
Published: June 18, 2019

REFERENCES

Ashton, T.M., Fokas, E., Kunz-Schughart, L.A., Folkes, L.K., Anbalagan, S., Huether, M., Kelly, C.J., Pirovano, G., Buffa, F.M., Hammond, E.M., et al. (2016). The anti-malarial atovaquone increases radiosensitivity by alleviating tumour hypoxia. Nat. Commun. *7*, 12308.

Ashton, T.M., McKenna, W.G., Kunz-Schughart, L.A., and Higgins, G.S. (2018). Oxidative Phosphorylation as an Emerging Target in Cancer Therapy. Clin. Cancer Res. *24*, 2482–2490.

Bell, E.L., Klimova, T.A., Eisenbart, J., Moraes, C.T., Murphy, M.P., Budinger, G.R., and Chandel, N.S. (2007). The Qo site of the mitochondrial complex III is required for the transduction of hypoxic signaling via reactive oxygen species production. J. Cell Biol. *177*, 1029–1036.

Birsoy, K., Wang, T., Chen, W.W., Freinkman, E., Abu-Remaileh, M., and Sabatini, D.M. (2015). An Essential Role of the Mitochondrial Electron Transport Chain in Cell Proliferation Is to Enable Aspartate Synthesis. Cell *162*, 540–551.

Bricker, D.K., Taylor, E.B., Schell, J.C., Orsak, T., Boutron, A., Chen, Y.C., Cox, J.E., Cardon, C.M., Van Vranken, J.G., Dephoure, N., et al. (2012). A mitochondrial pyruvate carrier required for pyruvate uptake in yeast, Drosophila, and humans. Science *337*, 96–100.

Chang, C.Y., Kazmin, D., Jasper, J.S., Kunder, R., Zuercher, W.J., and McDonnell, D.P. (2011). The metabolic regulator ERRα, a downstream target of HER2/IGF-1R, as a therapeutic target in breast cancer. Cancer Cell *20*, 500–510.

Chang, E., Liu, H., Unterschemmann, K., Ellinghaus, P., Liu, S., Gekeler, V., Cheng, Z., Berndorff, D., and Gambhir, S.S. (2015). 18F-FAZA PET imaging response tracks the reoxygenation of tumors in mice upon treatment with the mitochondrial complex I inhibitor BAY 87-2243. Clin. Cancer Res. *21*, 335–346.

Charest-Marcotte, A., Dufour, C.R., Wilson, B.J., Tremblay, A.M., Eichner, L.J., Arlow, D.H., Mootha, V.K., and Giguère, V. (2010). The homeobox protein Prox1 is a negative modulator of ERRalpha/PGC-1alpha bioenergetic functions. Genes Dev. *24*, 537–542.

Cheng, G., Zielonka, J., Ouari, O., Lopez, M., McAllister, D., Boyle, K., Barrios, C.S., Weber, J.J., Johnson, B.D., Hardy, M., et al. (2016). Mitochondria-Targeted Analogues of Metformin Exhibit Enhanced Antiproliferative and Radiosensitizing Effects in Pancreatic Cancer Cells. Cancer Res. *76*, 3904–3915.

Corbet, C., Bastien, E., Draoui, N., Doix, B., Mignion, L., Jordan, B.F., Marchand, A., Vanherck, J.C., Chaltin, P., Schakman, O., et al. (2018). Interruption of

lactate uptake by inhibiting mitochondrial pyruvate transport unravels direct antitumor and radiosensitizing effects. Nat. Commun. *9*, 1208.

Dang, C.V., Hamaker, M., Sun, P., Le, A., and Gao, P. (2011). Therapeutic targeting of cancer cell metabolism. J. Mol. Med. (Berl.) *89*, 205–212.

Dhani, N., Fyles, A., Hedley, D., and Milosevic, M. (2015). The clinical significance of hypoxia in human cancers. Semin. Nucl. Med. *45*, 110–121.

Di Lisa, F., and Ziegler, M. (2001). Pathophysiological relevance of mitochondria in NAD(+) metabolism. FEBS Lett. *492*, 4–8.

Diepart, C., Karroum, O., Magat, J., Feron, O., Verrax, J., Calderon, P.B., Grégoire, V., Leveque, P., Stockis, J., Dauguet, N., et al. (2012). Arsenic trioxide treatment decreases the oxygen consumption rate of tumor cells and radiosensitizes solid tumors. Cancer Res. *72*, 482–490.

Eichner, L.J., and Giguère, V. (2011). Estrogen related receptors (ERRs): a new dawn in transcriptional control of mitochondrial gene networks. Mitochondrion *11*, 544–552.

Ellinghaus, P., Heisler, I., Unterschemmann, K., Haerter, M., Beck, H., Greschat, S., Ehrmann, A., Summer, H., Flamme, I., Oehme, F., et al. (2013). BAY 87-2243, a highly potent and selective inhibitor of hypoxia-induced gene activation has antitumor activities by inhibition of mitochondrial complex I. Cancer Med. *2*, 611–624.

Fan, J., Ye, J., Kamphorst, J.J., Shlomi, T., Thompson, C.B., and Rabinowitz, J.D. (2014). Quantitative flux analysis reveals folate-dependent NADPH production. Nature *510*, 298–302.

Faubert, B., Li, K.Y., Cai, L., Hensley, C.T., Kim, J., Zacharias, L.G., Yang, C., Do, Q.N., Doucette, S., Burguete, D., et al. (2017). Lactate Metabolism in Human Lung Tumors. Cell *171*, 358–371.e9.

Gaillard, S., Grasfeder, L.L., Haeffele, C.L., Lobenhofer, E.K., Chu, T.M., Wolfinger, R., Kazmin, D., Koves, T.R., Muoio, D.M., Chang, C.Y., and McDonnell, D.P. (2006). Receptor-selective coactivators as tools to define the biology of specific receptor-coactivator pairs. Mol. Cell *24*, 797–803.

Ganapathy-Kanniappan, S., and Geschwind, J.F. (2013). Tumor glycolysis as a target for cancer therapy: progress and prospects. Mol. Cancer *12*, 152.

Gilkes, D.M., Semenza, G.L., and Wirtz, D. (2014). Hypoxia and the extracellular matrix: drivers of tumour metastasis. Nat. Rev. Cancer *14*, 430–439.

Gross, M.I., Demo, S.D., Dennison, J.B., Chen, L., Chernov-Rogan, T., Goyal, B., Janes, J.R., Laidig, G.J., Lewis, E.R., Li, J., et al. (2014). Antitumor activity of the glutaminase inhibitor CB-839 in triple-negative breast cancer. Mol. Cancer Ther. *13*, 890–901.

Gui, D.Y., Sullivan, L.B., Luengo, A., Hosios, A.M., Bush, L.N., Gitego, N., Davidson, S.M., Freinkman, E., Thomas, C.J., and Vander Heiden, M.G. (2016). Environment Dictates Dependence on Mitochondrial Complex I for NAD+ and Aspartate Production and Determines Cancer Cell Sensitivity to Metformin. Cell Metab. *24*, 716–727.

Haq, R., Shoag, J., Andreu-Perez, P., Yokoyama, S., Edelman, H., Rowe, G.C., Frederick, D.T., Hurley, A.D., Nellore, A., Kung, A.L., et al. (2013). Oncogenic BRAF regulates oxidative metabolism via PGC1α and MITF. Cancer Cell *23*, 302–315.

Herzig, S., Raemy, E., Montessuit, S., Veuthey, J.L., Zamboni, N., Westermann, B., Kunji, E.R., and Martinou, J.C. (2012). Identification and functional expression of the mitochondrial pyruvate carrier. Science *337*, 93–96.

Ho, P.C., Bihuniak, J.D., Macintyre, A.N., Staron, M., Liu, X., Amezquita, R., Tsui, Y.C., Cui, G., Micevic, G., Perales, J.C., et al. (2015). Phosphoenolpyruvate Is a Metabolic Checkpoint of Anti-tumor T Cell Responses. Cell *162*, 1217–1228.

Hui, S., Ghergurovich, J.M., Morscher, R.J., Jang, C., Teng, X., Lu, W., Esparza, L.A., Reya, T., Le Zhan, Yanxiang Guo, J., et al. (2017). Glucose feeds the TCA cycle via circulating lactate. Nature *551*, 115–118.

Jordan, B.F., and Sonveaux, P. (2012). Targeting tumor perfusion and oxygenation to improve the outcome of anticancer therapy. Front. Pharmacol. *3*, 94.

Liu, X., Ser, Z., and Locasale, J.W. (2014). Development and quantitative evaluation of a high-resolution metabolomics technology. Anal. Chem. *86*, 2175–2184.

Liu, L., Shah, S., Fan, J., Park, J.O., Wellen, K.E., and Rabinowitz, J.D. (2016a). Malic enzyme tracers reveal hypoxia-induced switch in adipocyte NADPH pathway usage. Nat. Chem. Biol. *12*, 345–352.

Liu, X., Romero, I.L., Litchfield, L.M., Lengyel, E., and Locasale, J.W. (2016b). Metformin Targets Central Carbon Metabolism and Reveals Mitochondrial Requirements in Human Cancers. Cell Metab. *24*, 728–739.

Luo, C., Balsa, E., Thomas, A., Hatting, M., Jedrychowski, M., Gygi, S.P., Widlund, H.R., and Puigserver, P. (2017). ERRα Maintains Mitochondrial Oxidative Metabolism and Constitutes an Actionable Target in PGC1α-Elevated Melanomas. Mol. Cancer Res. *15*, 1366–1375.

Muir, A., and Vander Heiden, M.G. (2018). The nutrient environment affects therapy. Science *360*, 962–963.

Norris, J.D., Chang, C.Y., Wittmann, B.M., Kunder, R.S., Cui, H., Fan, D., Joseph, J.D., and McDonnell, D.P. (2009). The homeodomain protein HOXB13 regulates the cellular response to androgens. Mol. Cell *36*, 405–416.

Pagliarini, D.J., and Rutter, J. (2013). Hallmarks of a new era in mitochondrial biochemistry. Genes Dev. *27*, 2615–2627.

Park, S., Chang, C.Y., Safi, R., Liu, X., Baldi, R., Jasper, J.S., Anderson, G.R., Liu, T., Rathmell, J.C., Dewhirst, M.W., et al. (2016). ERRα-Regulated Lactate Metabolism Contributes to Resistance to Targeted Therapies in Breast Cancer. Cell Rep. *15*, 323–335.

Safi, R., Nelson, E.R., Chitneni, S.K., Franz, K.J., George, D.J., Zalutsky, M.R., and McDonnell, D.P. (2014). Copper signaling axis as a target for prostate cancer therapeutics. Cancer Res. *74*, 5819–5831.

Sborov, D.W., Haverkos, B.M., and Harris, P.J. (2015). Investigational cancer drugs targeting cell metabolism in clinical development. Expert Opin. Investig. Drugs *24*, 79–94.

Schell, J.C., Olson, K.A., Jiang, L., Hawkins, A.J., Van Vranken, J.G., Xie, J., Egnatchik, R.A., Earl, E.G., DeBerardinis, R.J., and Rutter, J. (2014). A role for the mitochondrial pyruvate carrier as a repressor of the Warburg effect and colon cancer cell growth. Mol. Cell *56*, 400–413.

Schoors, S., Bruning, U., Missiaen, R., Queiroz, K.C., Borgers, G., Elia, I., Zecchin, A., Cantelmo, A.R., Christen, S., Goveia, J., et al. (2015). Fatty acid carbon is essential for dNTP synthesis in endothelial cells. Nature *520*, 192–197.

Shestov, A.A., Liu, X., Ser, Z., Cluntun, A.A., Hung, Y.P., Huang, L., Kim, D., Le, A., Yellen, G., Albeck, J.G., and Locasale, J.W. (2014). Quantitative determinants of aerobic glycolysis identify flux through the enzyme GAPDH as a limiting step. eLife *3*, e03342.

Skoura, E., Datseris, I.E., Platis, I., Oikonomopoulos, G., and Syrigos, K.N. (2012). Role of positron emission tomography in the early prediction of response to chemotherapy in patients with non–small-cell lung cancer. Clin. Lung Cancer *13*, 181–187.

Sonveaux, P., Végran, F., Schroeder, T., Wergin, M.C., Verrax, J., Rabbani, Z.N., De Saedeleer, C.J., Kennedy, K.M., Diepart, C., Jordan, B.F., et al. (2008). Targeting lactate-fueled respiration selectively kills hypoxic tumor cells in mice. J. Clin. Invest. *118*, 3930–3942.

Stein, L.R., and Imai, S. (2012). The dynamic regulation of NAD metabolism in mitochondria. Trends Endocrinol. Metab. *23*, 420–428.

Sullivan, L.B., Gui, D.Y., Hosios, A.M., Bush, L.N., Freinkman, E., and Vander Heiden, M.G. (2015). Supporting Aspartate Biosynthesis Is an Essential Function of Respiration in Proliferating Cells. Cell *162*, 552–563.

Trédan, O., Galmarini, C.M., Patel, K., and Tannock, I.F. (2007). Drug resistance and the solid tumor microenvironment. J. Natl. Cancer Inst. *99*, 1441–1454.

Urra, F.A., Muñoz, F., Lovy, A., and Cárdenas, C. (2017). The Mitochondrial Complex(I)ty of Cancer. Front. Oncol. *7*, 118.

Vacanti, N.M., Divakaruni, A.S., Green, C.R., Parker, S.J., Henry, R.R., Ciaraldi, T.P., Murphy, A.N., and Metallo, C.M. (2014). Regulation of substrate utilization by the mitochondrial pyruvate carrier. Mol. Cell *56*, 425–435.

Vander Heiden, M.G., and DeBerardinis, R.J. (2017). Understanding the Intersections between Metabolism and Cancer Biology. Cell *168*, 657–669.

Vazquez, F., Lim, J.H., Chim, H., Bhalla, K., Girnun, G., Pierce, K., Clish, C.B., Granter, S.R., Widlund, H.R., Spiegelman, B.M., and Puigserver, P. (2013). PGC1α expression defines a subset of human melanoma tumors with increased mitochondrial capacity and resistance to oxidative stress. Cancer Cell *23*, 287–301.

Vellinga, T.T., Borovski, T., de Boer, V.C., Fatrai, S., van Schelven, S., Trumpi, K., Verheem, A., Snoeren, N., Emmink, B.L., Koster, J., et al. (2015). SIRT1/PGC1α-Dependent Increase in Oxidative Phosphorylation Supports Chemotherapy Resistance of Colon Cancer. Clin. Cancer Res. *21*, 2870–2879.

Viale, A., Pettazzoni, P., Lyssiotis, C.A., Ying, H., Sánchez, N., Marchesini, M., Carugo, A., Green, T., Seth, S., Giuliani, V., et al. (2014). Oncogene ablation-resistant pancreatic cancer cells depend on mitochondrial function. Nature *514*, 628–632.

Weinberg, S.E., and Chandel, N.S. (2015). Targeting mitochondria metabolism for cancer therapy. Nat. Chem. Biol. *11*, 9–15.

Weinberg, F., Hamanaka, R., Wheaton, W.W., Weinberg, S., Joseph, J., Lopez, M., Kalyanaraman, B., Mutlu, G.M., Budinger, G.R., and Chandel, N.S. (2010). Mitochondrial metabolism and ROS generation are essential for Kras-mediated tumorigenicity. Proc. Natl. Acad. Sci. USA *107*, 8788–8793.

Wise, D.R., DeBerardinis, R.J., Mancuso, A., Sayed, N., Zhang, X.Y., Pfeiffer, H.K., Nissim, I., Daikhin, E., Yudkoff, M., McMahon, S.B., and Thompson, C.B. (2008). Myc regulates a transcriptional program that stimulates mitochondrial glutaminolysis and leads to glutamine addiction. Proc. Natl. Acad. Sci. USA *105*, 18782–18787.

Wolpaw, A.J., and Dang, C.V. (2018). Exploiting Metabolic Vulnerabilities of Cancer with Precision and Accuracy. Trends Cell Biol. *28*, 201–212.

Xiang, Y., Stine, Z.E., Xia, J., Lu, Y., O'Connor, R.S., Altman, B.J., Hsieh, A.L., Gouw, A.M., Thomas, A.G., Gao, P., et al. (2015). Targeted inhibition of tumor-specific glutaminase diminishes cell-autonomous tumorigenesis. J. Clin. Invest. *125*, 2293–2306.

Yang, C., Ko, B., Hensley, C.T., Jiang, L., Wasti, A.T., Kim, J., Sudderth, J., Calvaruso, M.A., Lumata, L., Mitsche, M., et al. (2014). Glutamine oxidation maintains the TCA cycle and cell survival during impaired mitochondrial pyruvate transport. Mol. Cell *56*, 414–424.

Yuan, J., Bennett, B.D., and Rabinowitz, J.D. (2008). Kinetic flux profiling for quantitation of cellular metabolic fluxes. Nat. Protoc. *3*, 1328–1340.

Yuk, J.M., Kim, T.S., Kim, S.Y., Lee, H.M., Han, J., Dufour, C.R., Kim, J.K., Jin, H.S., Yang, C.S., Park, K.S., et al. (2015). Orphan Nuclear Receptor ERRα Controls Macrophage Metabolic Signaling and A20 Expression to Negatively Regulate TLR-Induced Inflammation. Immunity *43*, 80–91.

Zannella, V.E., Dal Pra, A., Muaddi, H., McKee, T.D., Stapleton, S., Sykes, J., Glicksman, R., Chaib, S., Zamiara, P., Milosevic, M., et al. (2013). Reprogramming metabolism with metformin improves tumor oxygenation and radiotherapy response. Clin. Cancer Res. *19*, 6741–6750.

STAR★METHODS

KEY RESOURCES TABLE

REAGENT or RESOURCE	SOURCE	IDENTIFIER
Antibodies		
Rabbit monoclonal anti-ERRα	abcam	Cat#ab76228;RRID:AB_1523580
Rabbit polyclonal anti-PGC1α	Santa Cruz Biotechnolgoy	Cat#sc13067;RRID:AB_2166218
Mouse monoclonal anti-β-actin	Sigma-Aldrich	Cat#A2228;RRID:AB_476697
Rabbit monoclonal anti-MPC1	Cell Signaling Technology	Cat#14462;RRID:AB_2773729
Rabbit monoclonal anti-MPC2	Cell Signaling Technology	Cat#46141;RRID:AB_2799295
Rabbit monoclonal anti-VDAC	Cell Signaling Technology	Cat#4661;RRID:AB_10557420
Rabbit polyclonal anti-PDH-E1α(pSer293)	Sigma-Aldrich	Cat#AP1062;RRID:AB_10616069
Mouse monoclonal anti- PDH-E1α	Thermo Fisher Scientific	Cat#459400;RRID:AB_2532238
Chemicals, Peptides, and Recombinant Proteins		
Cpd29	This paper	N/A
BPTES	Selleckchem	Cat#S7753
CB-839	Selleckchem	Cat#S7655
MTX	Selleckchem	Cat#S1210
trans-DHEA	Sigma-Aldrich	Cat#D4000
Sodium L-Lactate	Sigma-Aldrich	Cat#71718
L-Glutathione reduced	Sigma-Aldrich	Cat#G6013
CM-H_2DCFDA	Thermo Fisher Scientific	Cat# C6827
D-glucose (U13C6)	Cambridge Isotope Laboratories	Cat#CLM-1396
L-glutamine (13C5)	Cambridge Isotope Laboratories	Cat#CLM-1822-H
Bacterial and Virus Strains		
β-gal adenovirus	Gaillard et al., 2006	N/A
PGC1α adenovirus	Gaillard et al., 2006	N/A
PGC1α_2X9 adenovirus	Gaillard et al., 2006	N/A
PGC1α_L2L3M adenovirus	Gaillard et al., 2006	N/A
Critical Commercial Assays		
NADP/NADPH-Glo™ Assays	Promega	Cat#G9071
Experimental Models: Cell Lines		
MDAMB436	ATCC	Cat#HTB-130
HCC1937	ATCC	Cat#CRL-2336
HCC1143	ATCC	Cat#CRL-2321
MDAMB231	ATCC	Cat#HTB-26
BT20	ATCC	Cat#HTB-19
BT549	ATCC	Cat#HTB-122
HCC1806	ATCC	Cat#CRL-2335
Oligonucleotides		
36B4-F qPCR primer: GGACATGTTGCT GGCCAATAA	IDT DNA	N/A
36B4-R qPCR primer: GGGCCCGAGAC CAGTGTT	IDT DNA	N/A
MPC1-F qPCR primer: TTATCAGTGGG CGGATGACAT	IDT DNA	N/A
MPC1-R qPCR primer: GCTGTACCTTG TAGGCAAATCTC	IDT DNA	N/A

(*Continued on next page*)

Continued

REAGENT or RESOURCE	SOURCE	IDENTIFIER
MPC1-F ChIP primer: CTTCTCCCGAG CACTTTCCC	IDT DNA	N/A
MPC1-R ChIP primer: AATGCTTTCCTC CTCCGACG	IDT DNA	N/A
siRNA for MDH1	Thermo Fisher Scientific	Cat#HSS106413
siRNA for G6PD-B	Thermo Fisher Scientific	Cat#HSS103892
siRNA for G6PD-C	Thermo Fisher Scientific	Cat#HSS103893
Stealth siLuc	Thermo Fisher Scientific	Cat#12935-146
siERRα-A: UGGUGGGCAUUGAGCCU CUCUACAU	Thermo Fisher Scientific	N/A
siERRα-B: GAAUGCACUGGUGUCUC AUCUGCUG	Thermo Fisher Scientific	N/A
Recombinant DNA		
psPAX	Addgene	Cat#12260
pCMB-VSV-G	Addgene	Cat#8454
LeGO-iG2-MPC1	Dr. Jared Rutter	N/A
LeGO-iC2-MPC2	Dr. Jared Rutter	N/A
LeGO-iG2	Addgene	Cat#27341
LeGO-iC2	Addgene	Cat#27345
Software and Algorithms		
GraphPad Prism	GraphPad Software, Inc	N/A
Integrative Genomics Viewer (IGV)	http://software.broadinstitute.org/software/igv	N/A
Other		
ChIP-seq data for ESRRA were downloaded from ENCODE database	https://www.encodeproject.org	N/A

CONTACT FOR REAGENT AND RESOURCE SHARING

Further information and requests for reagents may be directed to and fulfilled by the Lead Contact, Donald P. McDonnell (donald.mcdonnell@duke.edu).

EXPERIMENTAL MODELS AND SUBJECT DETAILS

Animals and In Vivo Procedures

Animals were maintained in accordance with the NIH Guide for Care and Use of Laboratory Animals, and all procedures were approved by the Duke University Institutional Animal Care and Use Committees. MDA436 cells (2.5×10^6) in 50% Matrigel (BD Biosciences) were injected into the mammary fat pad of 8-week-old female NOD.SCID.gamma (NSG) mice. When tumors reached 150 mm^3, mice were randomized and fed either control chow or chow containing Cpd29 (240 ppm), trans-DHEA (0.2%), CB-839 (0.28%) alone or in combination. This dose was calculated to deliver approximately 30 mg/kg/day (Cpd29), 250 mg/kg/day (t-DHEA), and 400 mg/kg/day (CB-839). Mice were maintained on this diet until they were euthanized. Tumor size was measured with calipers three times a week, and tumor volumes were calculated as ($width^2$ x length)/2. Statistical comparison among groups was carried out using two-way ANOVA followed by a Bonferroni multiple comparison test.

Cell Culture

All cell lines were obtained from ATCC (Manassas, VA) and maintained in a 37°C incubator with 5% CO_2. MDA-MB-436, HCC1937, HCC1143, HCC1806, and BT549 were cultured in RPMI (Thermo Fisher Scientific), and MDA-MB-231, and BT20 were cultured in DMEM (Thermo Fisher Scientific). All media were supplemented with 8% fetal bovine serum (Sigma), 1 mM sodium pyruvate and 0.1 mM non-essential amino acids (Thermo Fisher Scientific). Cells were re-fed with fresh media every three days. All lentiviral transductions were performed with second-generation lentiviral supernatants generated by cotransfection of 293T cells with vectors psPAX2 (Addgene #12260), pCMV-VSV-G (Addgene #8454), and lentiviral targeting vectors. The lentiviral targeting vectors (Lego iG2/iC2) harboring MPC1 and MPC2 were kindly provided by Dr. Jared Rutter, University of Utah School of Medicine

(Schell et al., 2014). MPC1/2-expressing stable MDA436 cell lines were generated by GFP and mCherry double positive cell sorting by flow cytometry. Cells were sorted three times over a period of 4 weeks until more than 98% of the cells were GFP/mCherry double positive.

METHOD DETAILS

Proliferation Assay

Breast cancer cells were seeded in 96-well plates containing regular RPMI or DMEM media for 48 hr and subsequently replaced with glucose and glutamine-free DMEM (10% dialyzed FBS) supplemented with 10 mM sodium lactate and 2 mM glutamine (glucose-deprived conditions) or 12.5 mM glucose and 2 mM glutamine (glucose-replete conditions). Cells were harvested 2, 4, 6, or 8 days after treatment. Cell numbers were determined by staining with the DNA dye Hoechst 33258 (Sigma) and resulting fluorescence was read at excitation 346 nm and emission 460 nm using a Fusion microplate reader (PerkinElmer).

U-^{13}C Glutamine and U-^{13}C Glucose Isotopomer Analysis

MDA436 (3.5×10^5 cells/well) cells were seeded in 6-well plates containing regular RPMI. After incubation at 37°C for 24 hr, cells were pre-treated with DMSO or 5 μM Cpd29 for 40 hr in regular RPMI. Cells were then washed with PBS and switched to glucose and glutamine-free DMEM (10% dialyzed FBS) supplemented with 10 mM lactate + 2 mM [U-^{13}C] glutamine (glucose-deprived conditions) or 12.5 mM [U-^{13}C] glucose + 2 mM glutamine or 12.5 mM glucose + 2 mM [U-^{13}C] glutamine (glucose-replete conditions) in the presence of DMSO or 5 μM Cpd29 and incubated for 24 hr. After 24 hr, media were quickly removed, and the plates were placed on top of dry ice. 1 mL of extraction solvent (80% methanol/water) was added, and the plates were transferred to −80°C freezer. The plates were left for 15 min, and then cells were scraped into extraction solvent on dry ice. The whole extracts were transferred to new microcentrifuge tubes and centrifuged at 20,000 g for 10 min at 4°C. The supernatants were transferred to new microcentrifuge tubes and dried in a SpeedVac. Dried samples were stored in −80°C freezer until LC-MS analysis. For relative metabolite levels, the total ion count measured by mass spectrometry was normalized to cellular protein for each sample and then plotted as relative to DMSO treatment. In addition, we corrected for naturally occurring 13C isotope as previously described (Yuan et al., 2008).

LC-MS Analysis

LC equipped with an Xbridge amide column (100 × 2.1 mm i.d., 3.5 μm; Waters) was coupled to Q Exactive mass spectrometer (Thermo Fisher Scientific). Cell extracts were reconstituted into 30 μL water:methanol:acetonitrile (2:1:1), and 3 μL was injected to LC-MS (Liu et al., 2014; Shestov et al., 2014). The peak area integration of every metabolite was done with manufacturer's software SIEVE (Thermo Fisher Scientific), and used to calculate isotopomer distribution. The natural abundance was corrected based on previously published method (Yuan et al., 2008). The contribution of carbon is calculated using the method described in a previous study (Schoors et al., 2015).

Quantitative PCR

Total DNA-free RNA was isolated using the Aurum RNA kit (Bio-Rad Laboratories, Hercules, CA) following the manufacturer's instructions. Using the Bio-Rad iScript kit, five hundred nanograms of total RNA were used in each 10 μL reverse transcription reaction, and the resulting cDNA was diluted 1:10 with water to use in qPCR analysis. qPCR was performed using the Bio-Rad SYBR green supermix with 0.2 μM of each forward and reverse primer and 1.25 μL of diluted cDNA in a total reaction volume of 3.25 μL. PCR amplification was carried out using the Bio-Rad CFX384 qPCR system.

Western Blot Analysis

Cell extracts were prepared using ice-cold lysis buffer [50 mM Tris-HCl (pH 7.4), 150 mM NaCl, 1% Nonidet P-40, 0.5% sodium deoxycholate, 0.05% sodium dodecyl sulfate, 100 mM NaF and 1 mM EDTA] supplemented with protease inhibitor cocktails (Sigma) and 1 mM Na_3VO_4 (Sigma). Protein concentrations were determined by the BCA protein assay (Thermo Fisher Scientific). 20 μg of proteins were separated on SDS-PAGE gels, transferred onto nitrocellulose membranes, and subjected to immunoblotting using the indicated antibodies. Blots were imaged with the Odyssey infrared imaging system (Li-Cor).

Chromatin Immunoprecipitation Assay (ChIP)

Chromatin immunoprecipitation assay was performed as previously described (Norris et al., 2009). MDA436 cells were plated in 150 mm dishes in regular RPMI for 48 hr. Cells were then transfected with either control (siCtrl) or ERRα (siERRα-A and siERRα-B) siRNAs for 24 hr, followed by infection of adenoviruses expressing β-gal (negative control), wild-type PGC-1α, ERRα selective PGC-1α (2X9), or the nuclear receptor-binding deficient PGC-1α (L2L3M) for 48 hr. 1% formaldehyde was added directly to the media for 10 min and quenched with 250 mM glycine for 5 min. Cells were washed with ice-cold PBS, pelleted, lysed in 1 mL RIPA buffer (50 mM Tris-HCl (pH 7.4), 150 mM NaCl, 1% Nonidet P-40, 0.5% sodium deoxycholate, 0.05% sodium dodecyl sulfate, and 1 mM EDTA) and sonicated. The sonicated cross-linked chromatin was diluted with 2.3 mL of RIPA buffer and precleared for 30 min with 100 μL of 50% protein A/G agarose slurry (sc-2003, Santa Cruz) containing 50 μg BSA and 20 μg salmon sperm DNA. 1 mL of precleared chromatin was incubated with control rabbit IgG or anti-ERRα for overnight at 4°C. 70 μL of 50% protein A/G agarose beads were added and

incubated for 2 hr at 4°C. Beads were washed 2 times sequentially with 1 mL of low-salt buffer (50 mM HEPES pH7.8, 140 mM NaCl, 1 mM EDTA, 1% Triton X-100, 0.1% sodium deoxycholate, 0.1% sodium dodecyl sulfate), high-salt buffer (same as low-salt with 500 mM NaCl), LiCl buffer (20 mM Tris-HCl pH 8.0, 1 mM EDTA, 250 mM LiCl, 0.5% Nonidet P-40, 0.5% sodium deoxycholate), and TE buffer (50 mM Tris-HCl pH 8.0 and 1 mM EDTA). Protein-DNA complexes were eluted with elution buffer (50 mM Tris-HCl pH 8.0, 1 mM EDTA, and 1% SDS) at 65°C twice for 15 minutes. Eluted protein-DNA complexes were reverse cross-linked in the presence of 0.25 M NaCl overnight at 65°C and further treated with 4 μL of 0.5 M EDTA and 1 μg of proteinase K (20 mg/mL) at 42°C for 1 hr. The DNA fragments were purified and eluted in 10 mM Tris-HCl pH 8.5 using the QIAquick PCR purification kit (QIAGEN) and further diluted with water and analyzed by real-time qPCR.

Adenoviral Transduction

Adenovirus expressing β-gal, PGC-1α, PGC-1α 2X9, or PGC-1α L2L3M were generated as described previously (Gaillard et al., 2006). MDA436 cells were infected at multiplicity of infection (MOI) of 50 for 48 hours.

$NADP^+$ and NADPH measurement

$NADP^+$ and NADPH were assessed using a modified version of manufacturer's instructions supplied with the NADP/NADPH-Glo™ Assay kit (Promega). Cells were plated and treated as done for proliferation assays. Media were removed and cells were extracted in 120 μL ice-cold lysis buffer (1% dodecyltrimethylammonium bromide (DTAB) in 0.2 N NaOH diluted 1:1 with PBS), and immediately frozen at −80°C. To measure $NADP^+$, 50 μL of sample was moved to PCR tubes containing 25 μL of 0.4 N HCl and incubated at 60°C for 15 min, where acidic conditions selectively degrade NADPH. To measure NADPH, 50 μL of sample was moved to PCR tubes and incubated at 75°C for 30 min where basic conditions selectively degrade $NADP^+$. Following incubations, samples were incubated at room temperature for 10 min and neutralized with 25 μL 0.5 M Tris base ($NADP^+$) or 50 μL of 0.25 M Tris in 0.2 N HCl (NADPH). Manufacturer's instructions were followed thereafter to measure $NADP^+$ and NADPH.

ROS Generation Assay

Treated cells were stained with the oxidation-sensitive dye CM-H_2DCFDA (3 μmol/L) for 60 min in PBS at 37°C, and the treatment was terminated by ice-cold PBS. Reactive oxygen species (ROS) generation was determined by FACS as described (Safi et al., 2014).

Apoptosis Assay

Treated cells were collected and double stained with Alexa Fluor 488 Annexin V and Sytox (Invitrogen) according to the manufacturer's instruction. Annexin V-positive cells were considered apoptotic, and their percentage of the total number of cells was calculated. Ten thousand events were collected for each sample using a BD Accuri C6 flow cytometry (BD), and data were analyzed using FlowJo software (TreeStar).

QUANTIFICATION AND STATISTICAL ANALYSIS

ChIP-seq data for ESRRA were downloaded through ENCODE database (https://www.encodeproject.org). Statistically significant binding peaks found in the ChIP-seq dataset were visualized using the Integrative Genomics Viewer (IGV) genome browser (http://software.broadinstitute.org/software/igv). Statistical significance was determined by the Student's t test or two-way ANOVA followed by a Bonferroni multiple comparison test using GraphPad Prism 6.0. p values < 0.05 were considered significant.